RNA-sequencing manifests the intrinsic role of MAPKAPK2 in facilitating molecular crosstalk during HNSCC pathogenesis

Sourabh Soni[1,3,#+], Prince Anand[1,3,+], Mohit Kumar Swarnkar[2], Vikram Patial[1,3], Narendra V. Tirpude[1,3], Yogendra S. Padwad[1,3,*]

[*]Corresponding author: Yogendra S. Padwad

Address: Pharmacology and Toxicology Lab, Dietetics and Nutrition Technology Division, CSIR-Institute of Himalayan Bioresource Technology, Palampur, Himachal Pradesh-176 061, India. Tel.: +91 1894 233339 Ext. 473. Fax: +91 1894 230433

E-mail address: yogendra@ihbt.res.in

Authors' information

[1]Pharmacology and Toxicology Laboratory, CSIR-Institute of Himalayan Bioresource Technology (CSIR-IHBT), Palampur-176061, India

[2]Biotechnology Division, CSIR-Institute of Himalayan Bioresource Technology (CSIR-IHBT), Palampur-176061, India

[3]Academy of Scientific and Innovative Research (AcSIR), Ghaziabad-201002, India.

Sourabh Soni: sourabhsoniplp@gmail.com

Prince Anand: princeanandsaharsa4u@gmail.com

Mohit Kumar Swarnkar: mohitks@ihbt.res.in

Vikram Patial: vikrampatial@ihbt.res.in

Narendra V. Tirpude: narendra@ihbt.res.in

*Yogendra S. Padwad: yogendra@ihbt.res.in

[#]Current address: Division of Pulmonary and Critical Care Medicine, Brigham and Women's Hospital, Department of Medicine, Harvard Medical School, Boston, MA 02115, USA. Email: ssoni4@bwh.harvard.edu

+ Authors contributed equally to the manuscript.

Abstract

Background: Transcriptome profiling has been pivotal in better comprehending the convoluted biology of tumors including head and neck squamous cell carcinoma (HNSCC). Recently, growing evidence has implicated the role of mitogen-activated protein kinase-activated protein kinase-2 (MAPKAPK2 or MK2) in many human diseases including tumors. MK2 has been recently reported as a critical regulator of HNSCC that functions *via* modulating the transcript turnover of crucial genes involved in its pathogenesis. Comprehensive MK2-centric transcriptomic analyses could help the scientific community to delve deeper into MK2-pathway driven mechanisms of tumor progression, but such studies have not yet been reported. Consequently, to delineate the biological relevance of MK2 and its intricate crosstalk in the tumor milieu, an extensive transcriptome analysis of HNSCC was conceptualized and effectuated with MK2 at the nexus.

Methods: In the current study, comprehensive next-generation sequencing-based transcriptome profiling was accomplished to ascertain global patterns of mRNA expression profiles in both *in vitro* and *in vivo* models of the HNSCC microenvironment. The findings of the RNA-sequencing analysis were cross-validated *via* robust validation using nCounter gene expression assays, immunohistochemistry, and real-time quantitative polymerase chain reaction (RT–qPCR).

Results: Transcriptomic characterization followed by annotation and differential gene expression analyses identified certain MK2-regulated candidate genes constitutively involved in regulating HNSCC pathogenesis, and the biological significance of these genes was established by pathway enrichment analysis. Additionally, advanced gene expression assays through the nCounter system in conjunction with immunohistochemical analysis validated the transcriptome profiling outcomes quite robustly. Furthermore, the results obtained from immunohistochemistry and transcript stability analysis indicated the crucial role of MK2 in the modulation of the expression pattern of these genes in HNSCC tumors and cells.

Conclusions: Conclusively, the findings have paved the way toward the identification of new effective tumor markers and potential molecular targets for HNSCC management. The results have accentuated the importance of certain differentially expressed MK2-regulated genes that are constitutively involved in HNSCC pathogenesis to potentially serve as putative candidates for future endeavors pertaining to diagnosis and therapeutic interventions for HNSCC.

Keywords

Head and neck squamous cell carcinoma, Transcriptome, Mitogen-activated protein kinase-activated protein kinase-2, Differentially expressed genes, Pathogenesis, RNA-sequencing.

1. Background

Multifaceted regulatory networks tend to connect genes within a myriad of cellular processes. A plethora of genes are involved in fundamental biological processes such as cell differentiation, growth, and programmed cell death, and their role in many diseases is presently known [1]. However, the apprehension of their roles at a global level is still incomplete. Gene transcription and regulatory networks in conjunction with new genome-wide approaches have garnered huge attention in the pretext of gene regulation. Nevertheless, post-transcriptional mechanisms such as transcript stability are also highly crucial and require intricate regulation *via* a multitude of intracellular signaling pathways [2, 3]. In particular, the modulation of transcript stability through phosphorylation-mediated regulation of RNA-binding proteins (RBPs) by mitogen-activated protein kinases (MAPKs) has been a topic of great interest [2, 3, 4, 5].

Head and neck squamous cell carcinoma (HNSCC) having an incidence rate of ~600,000 cases yearly, is the seventh most common cancer worldwide and one of the most lethal cancers with an overall mortality rate of 40-50% [6,7]. HNSCCs are classified either histologically [8] or *via* the analysis of global transcription that employs etiology-specific

profiles [9, 10]. However, when these parameters were used for patient clustering, specific differences were observed in the clinical behavior of patients as well as their response to therapy [11]. The survival rates of HNSCC patients have not improved much, hence, HNSCC has been rightly termed a malignant tumor with a low survival rate [12]. Consequently, augmented mechanistic insight into the molecular basis of HNSCC pathogenesis is urgently required to help in the early diagnosis and development of effective therapeutics aimed at improved clinical outcomes [13].

The role of differentially expressed genes (DEGs) and endogenous RNA networks in HNSCC is not fully deciphered. Past reports on genome and transcriptome studies in various human tumors have revealed aberrant regulatory programs, driver mutations, and disease subtypes [14]. The cancer genome study is a valuable tool for classification, diagnosis, and prognosis in HNSCC. There have been many past reports pertaining to genomic alterations in HNSCC [15, 16]. Recently, The Cancer Genome Atlas (TCGA) has led to a global analysis of major molecular changes, a comprehensive landscape of transcriptomic alterations and pathogenesis-linked signaling pathways in tumors, thus, contributing to the identification of novel prognostic biomarkers or specific anticancer molecular targets [17, 18]. However, there is still a need for extensive research insights to decipher the prognostic value attributed to these genomic alterations in tumors such as HNSCC. A variety of biomarkers such as MAPK phosphatase-1 (MKP-1), p16, p27, p53, tumor necrosis factor-α (TNF-α), and vascular endothelial growth factor (VEGF) have been shown to be linked with HNSCC [5, 19], but they have not been proven to be sufficient in accurately defining HNSCC pathogenesis. Single biomarkers have generally proven insufficient in the prediction of therapeutic response thereby necessitating research on combinatorial markers through high-resolution “omics” profiling [20]. Consequently, the identification of reliable molecular biomarkers associated with HNSCC using omics-based analyses is needed to develop novel potential diagnostic and therapeutic targets [21].

Recently, the mRNA regulatory networks involved in tumor progression have garnered huge research interest with recent reports showing the role of these intricate networks in tumorigenesis [22]. However, research endeavors in this area are quite limited, thereby pointing to a pertinent need for comprehensive analyses of mRNAs and regulatory networks and their involvement in tumorigenesis. Next-generation sequencing (NGS) has rapidly evolved as an important tool for epigenomic, genomic, and transcriptomic profiling of cancers. Technological advances in mining and deciphering vast transcriptomic data have enabled us to better comprehend the complexity of various tumors and have streamlined efforts to discover novel biomarkers and therapeutic targets aimed at tumor management [23]. In a recent study, our team elucidated the role of mitogen-activated protein kinase-activated protein kinase-2 (MAPKAPK2 or MK2) in HNSCC pathogenesis using clinical tissue samples, cell lines, and heterotopic xenograft mouse model [5]. MK2 was found to be critically important in regulating HNSCC *via* modulating the transcript stability of crucial pathogenesis-related genes. It was also established that MK2-knockdown attenuated tumor progression in a xenograft mouse model [5]. Thereupon, to delve deeper into the mechanistic role of MK2 and to decipher the molecular markers responsible for MK2-mediated changes in HNSCC pathogenesis, a comprehensive transcriptome profiling was performed and evaluated.

In the present study, the global mRNA expression profiles in HNSCC experimental model sets were evaluated using transcriptome analysis on the NovaSeq 6000 system (Illumina Inc., USA). The *in vitro* HNSCC cells, CAL27-$MK2_{WT}$ (wild-type) and CAL27-$MK2_{KD}$ (knockdown), cultured in normoxic or the tumor microenvironment mimicking hypoxic conditions comprised the first set. The *in vivo* heterotopic HNSCC xenograft bearing tumors from CAL27-$MK2_{WT}$ and CAL27-$MK2_{KD}$ cells in immunocompromised mice (as described previously [5] formed the second set. Comprehensive transcriptome analysis in the experimental models highlighted certain specific MK2-mediated DEGs and regulatory

networks that play an integral role in HNSCC pathogenesis. Furthermore, specific gene expression assays on the nCounter system (NanoString Technologies, Inc., USA) were carried out to obtain a sensitive, highly multiplexed, and reliable detection of the defined mRNA targets based on the initial transcriptome profiling. The assays yielded highly precise and reproducible data that confirmed the transcriptome findings and yielded three MK2-regulated candidate genes (IGFBP2, MUC4, and PRKAR2B) intrinsically involved in HNSCC pathogenesis. Finally, cross-validation of the nCounter assay results in an *in vitro* setting, using immunohistochemistry (IHC) and mRNA transcript stability experiments through real time-quantitative polymerase chain reaction (RT-qPCR) was performed and it was found that these MK2-downstream genes showed dependence on MK2 for their expression and regulation in HNSCC tumors and cells (Figure 1). The findings corroborated recently published results, hence, ascertaining a crucial role of MK2 in HNSCC pathogenesis by means of transcript stability regulation [5]. These outcomes could potentially aid in the discovery of novel molecular markers for HNSCC management and diagnostic benefits.

2. Materials and Methods

2.1 Cell Culture

Homo sapiens tongue squamous cell carcinoma cell line CAL27 (CRL-2095™, ATCC, USA) was grown in specific media supplemented with 10% fetal bovine serum and 1% antibiotic-antimycotic (Gibco, USA). The cells were cultured under normal conditions (37°C, 5% CO_2 incubator with 95% humidity) and were free from any kind of contamination. Furthermore, MK2-specific short hairpin RNA-green fluorescent protein (shRNA-GFP) constructs were used to stably knockdown MK2 in cultured CAL27 cells to generate CAL27-$MK2_{KD}$ cells as previously described [5]. For hypoxia exposure, the cultured cells were seeded into Petri plates and incubated in 0.5% O_2 at 37°C in a hypoxia chamber for 48 hours (Bactrox, Shel-Lab, USA).

2.2 Xenograft mice model generation

To mimic the human tumor microenvironment, a biologically relevant heterotopic xenograft model of HNSCC was developed in non-obese diabetic/severe combined immunodeficient (NOD/SCID) mice. The immunocompromised mice were randomly assigned into control ($CAL27\text{-}MK2_{WT}$) and experimental ($CAL27\text{-}MK2_{KD}$) groups based on the specific cell type injected [5]. Briefly, for xenograft generation, $1x10^6$ cultured cells suspended in 100 µl of 1x phosphate buffered saline were injected subcutaneously into the right flanks of mice. Seven weeks post-graft inoculation, the mice were euthanized by CO_2 asphyxiation; tumors were aseptically excised, weighed, and used for tissue embedding or RNA isolation.

2.3 RNA extraction and sample preparation for RNA-sequencing (RNA-seq)

$CAL27\text{-}MK2_{WT}$ and $CAL27\text{-}MK2_{KD}$ cells cultured in normoxia/hypoxia and tumors resected from the xenografted mice were employed for isolation of total cellular RNA using the RNeasy Mini kit (Qiagen, Germany) following the manufacturer's recommended protocol (sample details are provided in Table 1). Consequently, the qualitative and quantitative assessment of all the RNA samples was performed using a NanoDrop 2000C spectrophotometer (Thermo Fisher Scientific, USA) and Bioanalyzer (Agilent 2100, Agilent Technologies, USA) (Figure S1). The RNA integrity number (RIN) value >5 was used as an exclusion criterion for this study. RNA samples having RIN>5 was used for cDNA library preparation. For each sample, RNA was isolated from at least three biological replicates for library construction and further experimentation.

2.4 cDNA library preparation and sequencing

Total RNA (5 µg) from each sample was used to isolate poly-A mRNA followed by preparation of cDNA library using the TruSeq mRNA sample preparation kit v2 (Illumina Inc.). Each sample was tagged with a unique TruSeq index tag to prepare multiplexed libraries. Six paired-end adapters with unique six base index sequences, permitting accurate

differentiation among samples, were used for the library preparation. The quantification of prepared libraries was performed on a Qubit fluorometer using a Qubit dsDNA BR assay kit (Life Technologies, USA), while the size and purity of the libraries were examined on a Bioanalyzer DNA 1000 series II chip (Agilent Technologies). The flow chart of the sequential steps involved in the TruSeq library preparation is given in Figure S2. The libraries (4 from the cell line model and 2 from the animal model) had an average insert size of 210 base pairs (bp) and were pooled by taking 10 µl from each library. The final pool was loaded in one lane of an S2 flow cell using the NovaSeq XP protocol (Illumina Inc.) (Figure S3) [24]. Cluster amplification and generation of sequencing data were performed on the NovaSeq 6000 system (Illumina Inc.) using 2x100 paired-end cycles. Raw data quality control was accomplished using the NGSQC tool kit v2.3 with default parameters [25].

2.5 Reference-based assembly and homology search

The raw FASTQ files with low-quality reads of sequencing data were filtered to obtain high-quality filtered data that were aligned to the reference genome (genome reference consortium human build 38 patch release 12, GRCh38.p12). The Kallisto pipeline was used for alignment and identification of transcript coding regions followed by quantitation and annotation using default parameters [26][27]. Furthermore, the removal of multi-mapped reads was performed, and the filtered data were finally converted to read counts for annotated genes. Figure 2a is a flowchart representation of the various steps involved in the sequencing data analyses.

2.6 Annotation, differential gene expression, and pathway analyses

Expression of the transcripts in the samples was analyzed based on their fragments per kilobase of transcript per million mapped (FPKM) values [26]. Transcripts were given a score for their expression by the Cufflinks-based maximum likelihood method and values with FPKM≥0.1 were considered significant for downstream analysis. Although FPKM≥0.1 cut-off indicates a low level of transcript expression, this value was essentially used to attain a

high enough threshold for the number of transcripts in the analyzed datasets considering the downstream filter-specific analyses performed in this study. Transcripts uniquely expressed in each sample were considered specific and were analyzed separately. The false discovery rate (FDR) was employed to correct the statistical significance of the p-values for multiple tests. DEGs in the analyzed datasets were identified *via* the DESeq analysis pipeline [27] using a fold change (FC) threshold of absolute log2 FC≥2 and a statistically significant Student's t-test p-value threshold adjusted for FDR<0.001. Consequently, transcripts with FC<-2 were considered downregulated while those with FC>2 were considered upregulated. Statistically, significant enriched functional classes with a p-value adjusted for FDR>0.05, derived using the hypergeometric distribution test corresponding to the DEGs, were determined using Student's t-test with the Benjamini Hochberg FDR test.

Unsupervised hierarchical clustering of DEGs was performed using Cluster 3.0 and visualized using Java TreeView [28, 29]. Gene ontology (GO) and pathways that harbor expressed transcripts were identified using the DAVID functional annotation tool (http://david.abcc.ncifcrf.gov/home.jsp) [28, 29, 30] (Figure 2a). For the DEGs, heat maps and volcano plots were generated using the 'gplots' and 'heat map' packages. GO and Kyoto Encyclopedia of Genes and Genomes (KEGG) pathway analyses were performed for the assembled transcripts with reference to the UniProt database. Data of the total DEGs (upregulated and downregulated) were explored further using Cytoscape v3.5.0 (http://www.cytoscape.org/) to better understand the gene regulatory networks and for mapping of the results [31]. In figures depicting the gene regulatory networks, the gene nodes/circles are sized according to their p-values and colored according to their FC where red shows upregulation, green depicts downregulation, and yellow displays baseline expression; processes are shown in rectangular boxes and colored in blue.

2.7 The nCounter gene expression assays for primary validation

To validate the leads obtained from the transcriptomic profiling, custom-designed molecular barcodes (NanoString Technologies, Inc.) were utilized for single-molecule imaging, thereby making it possible to detect and count hundreds of different transcripts in one reaction (Figure 1 and S4). RNA quality was assessed using the Agilent 2100 Bioanalyzer (Agilent Technologies) (Figure 1 and S1). Gene expression was analyzed on the nCounter system (NanoString Technologies, Inc.) following the manufacturer's recommendations. Briefly, the custom synthesized probes were hybridized overnight to the target RNA followed by washing away of the excess probes, immobilization of the CodeSet/RNA complexes in the nCounter cartridge, and finally data collection on the nCounter system (Figure 1 and S4). The gene expression levels were measured in triplicate for total RNA from the cell line and xenografted tumor samples, normalized to the four housekeeping genes (HKGs), and analyzed using nSolver software (NanoString Technologies, Inc.). Each nCounter assay contained synthetic spike-in controls in the preparatory mix to allow correction of the sample-to-sample variation arising due to common experimental errors such as differences in the amount of input transcripts or reagents [32]. The counts were normalized to the positive controls and averaged for the samples of each mRNA type. Normalization involved spiked-in positive and negative control probes for background correction in addition to the 4 HKGs. Data analyses were performed on the nSolver 3.0 analysis software (NanoString Technologies, Inc.).

2.8 Immunohistochemical analysis for secondary validation

The levels of expression and activation status of specific proteins were analyzed using IHC in the tumor sections from the *in vivo* xenograft model to validate the findings of the transcriptomic and the nCounter gene expression analysis. The animal study was approved by the Institutional Animal Ethics Committee (IAEC) of CSIR-IHBT, Palampur, India (Approval No. IAEC/IHBT-3/Mar 2017). IHC was performed according to the previously reported protocol [5]. Briefly, 5 µm thin sections fixed on poly-l-lysine coated slides were

deparaffinized and rehydrated. Antigen retrieval was performed using sodium citrate buffer (pH 6.0) followed by quenching of endogenous peroxidases using BLOXALL^{TM} blocking solution (Vector Laboratories, Inc., USA). Furthermore, incubation of the sections with 2.5% normal horse serum blocked the exposed sites. Sections were then incubated with appropriately diluted specific primary antibody (Table ST1) overnight at 4°C followed by horseradish peroxidase-conjugated secondary antibody for 1 hour at room temperature. The rinsed sections were then incubated with 3,3'-diaminobenzidine substrate and Mayer's hematoxylin served as a counterstain. Five field views were obtained from each section for the designated antibodies and used for quantitative analysis of protein expression.

2.9 Gene expression analysis and MK2-regulated transcript stability

To determine the role of MK2 in regulating transcript stability, the expression levels of selected genes and the stability of their transcripts were assessed in the presence/absence of MK2 using RT-qPCR in CAL27 cells. shRNA constructs were used to generate CAL27-$MK2_{KD}$ cells as previously reported [5]. MK2-knockdown was confirmed using western blotting (WB), following which CAL27-$MK2_{WT}$ and CAL27-$MK2_{KD}$ cells were treated with 1 µM actinomycin-D (Act-D) to inhibit transcription. Total RNA was isolated at 6 time points (0, 0.5, 1, 2, 4, and 8 hours) using the RNeasy Mini kit (Qiagen) according to the manufacturer's recommended protocol. The purity of the isolated RNA was determined using a NanoDrop 2000C spectrophotometer (Thermo Fisher Scientific) and the 260/280 ratios were found to be between 1.9 and 2.1. Further RT-qPCR was performed using a Verso 1-step RT-qPCR kit (Invitrogen, USA) as previously described [5]. GAPDH was used as an internal gene control and the difference in cycle threshold (Ct) was calculated following the $2^{-\Delta\Delta Ct}$ method. The relative fold change was calculated by comparing the CAL27-$MK2_{KD}$ (designated as shMix group, cells were treated with a combination of an equal amount of MK2 targeting shRNA complexes 1, 2, 3, and 4) at the 6 mentioned time points with CAL27-

$MK2_{WT}$ (designated as mock or scramble control group, cells were treated with scrambled shRNA). shRNA constructs and vector maps have been described previously [5].

2.10 Statistical analysis and quantification

All the experiments were conducted at least in triplicates unless mentioned otherwise. IHC staining intensity was observed and analyzed by an expert pathologist in a single-blinded fashion using a BX53 bright field microscope (Olympus Corporation, Japan). Quantification of protein expression for IHC and WB was performed using ImageJ software 1.8.0 (https://imagej.nih.gov/ij/). The images were RGB stacked, and the color threshold was adjusted according to the expression of specific proteins in the tissue section. For quantification, the expression was presented as a composite score of the percent area of the total tissues using ImageJ software. The statistical/imaging parameters used for the various transcriptomic analyses have been detailed with their explanations in their respective sections in the manuscript. GraphPad Prism 7.0 software (GraphPad Software, Inc., USA) was used for the data analysis of IHC and RT-qPCR quantified datasets.

3. Results

3.1 Qualitative assessment of the generated cDNA library followed by filtering and assembly of reads depicted optimum alignment

The quality assessment of the isolated total-RNA from the appropriate cells/tissues, as well as the cDNA library generated, was performed using a Bioanalyzer (Agilent 2100, Agilent Technologies). It was found that the RIN values of all the RNA samples and the cDNA library were >5 suggesting that they were of suitable quality for use in downstream experiments (Figure S1 and S3).

Deep sequencing of RNA obtained from the NovaSeq 6000 platform (Illumina Inc.) resulted in 349 million raw reads (~58.2 million raw reads per sample) with an average insert size of 210 bp. Figure S5 and S6 summarizes the quality check (QC) results of the

sequencing experiment. The raw FASTQ sequences were filtered using the NGSQC tool kit to obtain high-quality (HQ) reads based on the predefined parameters, generating 258 million filtered HQ reads (~43.1 million HQ reads per sample). This amounted to 74.1% of the total raw reads, implying that the obtained data were of good quality. A total of 25.7 gigabases of data were generated which enumerates the enormity and wide complexity of the human genome.

The HQ reads obtained were further examined in the downstream analyses and mapped over the human reference genome. The alignment performed by employing the Kallisto pipeline was optimum with 88.7% of the HQ reads on average being mapped to the human reference genome (Figure 2a and S6).

3.2 Annotation and differential gene expression analyses revealed candidate genes

The present study was conducted using two distinct experimental datasets as mentioned in Figure 1 and Table 1. Using the criteria of FPKM≥0.1, 62791 expressing transcripts on an average were identified per sample, which further represented thousands of genes. A-D datasets depict the *in vitro* HNSCC cell line samples while F vs E illustrates the *in vivo* xenograft dataset. As detailed in Figure 1 and Table 1, analyses of $MK2_{KD}$ vs $MK2_{WT}$ in normoxia and the tumor core emulating the hypoxic niche were performed to obtain a comprehensive picture of the changes in the global gene expression pattern. The differential gene expression in the analyzed datasets was evaluated and a large pool of the DEGs, precisely 1403 in B vs A, 924 in D vs C, 1360 in D vs B, 1456 in C vs A, and 984 in F vs E were found as assessed by the predefined cutoff values. Figure 2b represents the total number of upregulated (FC>2) and downregulated (FC<-2) genes among all the DEGs in the analyzed datasets.

3.3 Pathway enrichment analysis revealed the biological significance of the findings

The multitude of DEGs in the transcriptome profiling datasets was implicated in hundreds of significant biologies/biological processes as summarized in Figure 2c. To gain further insight into the biological significance of the variations in gene expression and to attain a global picture of the molecular pathways possibly contributing to HNSCC pathogenesis, pathway enrichment analyses were performed using the KEGG database. The resultant integrated network analysis revealed the top biological processes enriched in the analyzed datasets. The top GO pathway analyses for the DEGs are depicted in Figure 2d. Notably, a significant percentage (~5%) of the total DEGs in the analyzed datasets belonged to the pathways involved in cancer progression (Figure 2d). The DEGs showing significant changes among various groups were then selected, followed by the generation of heat maps to assess the clustering of gene expression profiles among the analyzed datasets (Figure 2e). Figure 2f further depicts the distribution of all the transcripts on the two dimensions of -log(P) and FC by way of volcano plots with differentially expressed transcripts highlighted in blue.

In the A-D datasets, the DEGs belonged to a multitude of biological processes thereby limiting the information that could be harnessed. Henceforth, to filter down the data to attain meaningful outcomes and fulfill the aim of extracting valuable leads, the 77 elements/biological processes that were common in A-D datasets were selected using Venny 2.1.0 (http://bioinfogp.cnb.csic.es/ tools/) (Figure 2g). These processes belonged to the various categories listed in Table ST2. Based on this knowledge, the common genes in these 77 biological processes were further filtered down using the same approach (Figure 2h). Consequently, 5 genes common in the A-D datasets were obtained namely death-associated protein 3 (DAP3), EH domain binding protein 1 (EHBP1), inositol hexakisphosphate kinase 2 (IP6K2), runt related transcription factor 1 (RUNX1), and SMC5-SMC6 complex localization factor 2 (SLF2) as listed in Table ST3. It is worth mentioning here that these MK2-regulated genes portray essential roles in HNSCC pathogenesis [33, 34, 35, 36]. Hence, further

exploratory investigations of these putative molecular targets are deemed essential for elucidating their relevance in HNSCC management.

3.4 Gene regulatory networks and pathways depicted the significance of the candidate genes in HNSCC pathogenesis

Gene regulatory networks for the 5 common genes in A-D datasets furnished a detailed overview of the various inter-network connections and the biological processes affected by them. Collectively, the results showed that DAP3 plays an intrinsic role in apoptosis and poly(A)-RNA binding while IP6K2 plays a role in ATP, nucleotide, and protein binding as confirmed in past reports [19, 32]. These genes showed differential regulation in *in-vitro* dataset (B vs A) hence, clearly signifying that MK2-knockdown, as well as the hypoxic tumor microenvironment, affects the genes and pathways *via* differential regulation, pointing to a central role of MK2 in transcriptional regulation of HNSCC. Interestingly, the *in-vitro* results published by our group recently [5] also pointed to the role of MK2 in modulating the transcript stability of MK2-regulated genes. Similarly, the xenograft dataset (F vs E) potentiated this finding (Figure 3a, 3b).

Furthermore, to retrieve the information pertaining to the MK2-regulated candidate genes intrinsic to HNSCC pathogenesis, the data were narrowed down to include only processes that were involved in tumor progression for further analysis. This filtering down the dataset to 16 cancer-specific biological processes that were common in the A-D datasets (listed in Table ST4). In these 16 processes only 2 genes, DAP3 and RUNX1, were found to be common based on the analysis performed using Venny 2.1.0 (Figure 2i and Table ST5). Collectively, these findings clearly indicated that DAP3 and RUNX1 were differentially expressed in the cell line-based datasets analyzed, hence, potentiating their intrinsic involvement in HNSCC pathogenesis and warranting further investigation. Notably, the 16 processes were found to be clustered in 5 major biological pathways (Figure S7) including

apoptosis and transcription, thereby, clearly showing that MK2 portrays an intrinsic role in the hypoxic tumor microenvironment by regulating these processes, hence, substantiating the latest *in vitro* findings from our group [5].

Similarly, on comparing the mice bearing CAL27-$MK2_{KD}$ tumors with those bearing CAL27-$MK2_{WT}$ tumors (F vs E xenograft dataset), it was found that the DEGs were clustered in 14 biological processes relevant to tumor pathogenesis as listed in Table ST6. The genes involved in these biological processes were assessed and Figure 3b shows the gene regulatory network. This analysis provided certain MK2-regulated candidate genes, such as TRAF2 [34] (apoptosis); EPB41L1 [35] (cytoskeleton); FOXO3, H2AFY and YAP1 (transcriptional regulation) [36] [37] [38]; and DIDO1 (RNA binding) [39] which are involved in key cellular processes in the xenograft model (Figure 3b). These findings can be explored further to decipher the putative role of the potential candidate genes in HNSCC pathogenesis with an aim to define the probable therapeutic targets for HNSCC management.

3.5 MK2 is the master of regulatory networks and functions by modulating transcript stability

The prime objective of this study was to gather comprehensive information regarding the various MK2-regulated DEGs and pathways that render essential roles in HNSCC pathogenesis in normoxic and tumor core mimicking hypoxic conditions. Thereupon, keeping MK2 at the nexus of further analyses, this study focused on elucidating the regulation of the MK2 pathway and its downstream targets in the analyzed datasets. MK2 was found to be involved in the regulation of major biological pathways as shown in Figure S7 and S8. Recent findings by our group have asserted that MK2 controls the transcript stability of critical genes involved in HNSCC pathogenesis *via* RBP-mediated regulation [5]. Hence, we further analyzed the transcriptomic data to decipher the role of MK2 in the regulation of mRNA stability. Interestingly, MK2 was found to accomplish this task through RBP-

mediated regulation with HuR (ELAVL1) and TTP (ZFP36) playing intrinsic roles (Figure 4a), thus, clearly affirming the hypothesis and corroborating previous findings [5]. The levels of expression of these RBPs and hence regulation varied in the analyzed datasets, thereby, clearly suggesting that the tumor microenvironment, in association with the presence/absence of MK2, plays an important role in HNSCC pathogenesis.

Next, to attain a clear understanding of what was happening at the transcriptional level, the analysis was narrowed down by selecting specific genes of the MK2 pathway. The genes were selected by literature mining of past MK2-centric studies and included those that were analyzed in our recent study [5]. Interestingly, the genes selected for this analysis, viz. AUF1, CEBPδ, CUGBP1, HuR, MK2, MKP-1, p27, p38, TNF-α, TTP, and VEGF, have been previously shown to be involved in several key cellular processes [reviewed in [4]. Elucidation of the MAPK signaling cluster in detail indicated that in the background of MK2-knockdown in normoxia (B vs A dataset), TNF-α and VEGF tended to show downregulation (Figure 4b), which is in complete consonance with previously published results. The analyzed genes were clustered into 6 major biological processes as shown for (F vs E xenograft dataset) in Figure 4c and Figure S8. Collectively, the results of the transcriptomic analysis corroborated very well with previous findings, thereby, robustly verifying the hypothesis that MK2 is the master regulator of the transcript stability of genes critical to HNSCC pathogenesis.

3.6 3'-untranslated region (3'-UTR)-based filtering furnished information regarding important MK2-regulated downstream target genes

In the present study, we focused on the role of MK2 and MK2-regulated genes in HNSCC pathogenesis. It is well known that MK2 can potentially regulate the transcript stability of only those downstream targets that possess binding regions for RBPs in their 3'-UTRs [40]. Hence, the transcriptomic analysis was narrowed down to only those DEGs that harbored

RBP-binding regions in their 3'-UTRs (Figure 5), an approach that has lately been the cornerstone of many 'omics' studies [41, 42, 43]. The DEGs were filtered based on the presence of adenylate-uridylate-rich elements (ARE)-regions in their 3'-UTRs where RBPs can potentially bind and modulate their function possibly *via* MK2-mediated regulation. To accomplish this task, the 3'-UTR regions of all the DEGs were fetched using Ensembl (http://www.ensembl.org/) [44]. Next, the domain sequences of RBPs were assessed using the catalog of inferred sequence binding preferences of the RBPs (CISBP-RNA) database [45]. Last, the transcripts that harbor RBP-specific regions in their 3'-UTRs were filtered out using the RBPmap v1.1 web tool (http://rbpmap.technion.ac.il/) (Figure 5a) [46]. Once the probable MK2-downstream targets were identified (based on the aforementioned approach), the data were reassessed focusing on the 16 previously selected cancer-specific pathways in the *in vitro* HNSCC cell line model (A-D datasets) (Table ST4). The top 2 upregulated and downregulated genes in this dataset were evaluated following 3'-UTR filtering which yielded 34 putative MK2-regulated genes as listed in Table ST7 (Figure 5b). Similarly, the topmost upregulated and downregulated genes were analyzed in all the cancer-specific pathways for the *in vivo* heterotopic HNSCC xenograft dataset (F vs E dataset) which provided 48 MK2-regulated genes that are listed in Table ST8 (Figure 5c). Collectively, this 3'-UTR-specific filtering of the transcriptomic data brought into the limelight possible MK2-downstream target genes that could be integral in HNSCC pathogenesis. Furthermore, to cross-validate the findings of the transcriptomic profiling, these candidate genes along with the 5 common genes in the 77 common elements in A-D datasets (listed in Table ST3) were used for further *in vitro* validation. H2AFY was common in the transcriptomic analysis for both the cell line and xenograft analysis (Table ST7 and ST8). Resultingly, a total of 86 genes (Table ST9) (34 MK2-regulated genes and 5 common genes for the A-D datasets, 48 MK2-regulated genes in the F vs E dataset, and the common gene, H2AFY, were counted once) were selected for further experimental validation (Figure 1).

3.7 Highly efficient and precise detection of gene expression *via* nCounter gene expression assays potentiated transcriptomic outcomes

Routinely, the findings of transcriptomic analyses are generally validated in an *in vitro* setting *via* gene expression analysis (employing RT-qPCR) using the same RNA sample to maintain homogeneity. In lieu of the high-throughput nature of the validation in this study, RT-qPCR analysis could have been very tedious and prone to numerous errors. Hence, as a viable and more pragmatic alternative, the latest and highly precise gene expression assay-based nCounter system approach (NanoString Technologies, Inc.) was employed to validate the outcomes of the transcriptome analysis in this study. To accomplish this, 90 specific custom-designed molecular probes corresponding to the selected MK2-regulated candidate genes were procured to aid in the imaging and fast detection of multiple transcripts (90 in this study) in a single reaction with a high-fidelity rate (NanoString Technologies, Inc.). The gene set comprised 86 selected genes from the transcriptomic profiling as well as 4 HKGs (listed in Table ST9 and ST10, respectively). 4 commonly used reference genes, viz. ABCF1, GAPDH, POLR2A, and RPL19, were selected based on an extensive literature survey and because of their baseline expression in both HNSCC as well as in MK2-knockdown conditions [47, 48].

The assay was performed using the standard procedure as highlighted in Figure S4 and S9 and detailed in the methods section. Briefly, the custom synthesized probes were hybridized to the target RNA samples followed by washing off the excess probes. Further, immobilization of the probe/RNA complexes on the nCounter cartridge was performed, samples were run on the nCounter instrument followed by data retrieval (NanoString Technologies, Inc.). Some of these genes were differentially expressed in the analyzed datasets as indicated by the statistical analysis ($p<0.05$). Next, to make sense of the biological significance of changes in gene expression in the nCounter data, KEGG pathway enrichment analysis was performed that revealed the top 5 biological processes (Figure 6a and 6b).

Furthermore, heat map analysis deciphered the clustering of the gene expression profiles among the various datasets (Figure 6c). The results from the nCounter assays correlated with the transcriptomic analysis (Table 2, 3 and 4), hence substantiating the findings.

Individually, the expression profile and variation in FC among the DEGs in the nCounter analysis in the *in vitro* CodeSet of 39 genes (Table ST3 and ST7) and in the *in vivo* CodeSet of 48 genes (Table ST8) have been showcased *via* the heat-map representations in Figure 6d, respectively. The results depict the upregulated and downregulated DEGs in the nCounter assays and the results were in consonance with the transcriptomic profiling with a high percentage of genes showing a similar pattern of expression and even matching FC values as shown in Table 3 and 4. For the B vs A dataset, a total of 39 genes were analyzed, out of which 24 matched the transcriptomic analysis (61.6% matching score). The matched genes were then analyzed for FC and BRD2 was found to be the only upregulated gene (FC>2), while CLK2 was the only downregulated gene (FC<2). Similarly, a step-by-step comprehensive analysis of all the datasets was performed and 12 DEGs that were common in the transcriptomic and nCounter analysis were revealed (the results are summarized in Table 2). Notably, these genes are key players in important processes such as apoptosis, cell cycle progression, and transcription regulation, hence, potentiating their role as important MK2-regulated genes involved in HNSCC pathogenesis (Figure 7d). Therefore, these results strengthen our recent findings that MK2 is critically important in regulating HNSCC and functions by modulating the transcript stability of crucial genes driving pathogenesis. Furthermore, detailed statistical analysis accentuated that the expression of only 7 (BMP7, CREB3L1, IGFBP2, MELK, MUC4, PRKAR2B, and ZNF662), out of the 12 candidate genes were significantly different among the datasets (FC>2 or <-2, $p<0.05$) (Table 2, 3, and 4). MELK was the only gene belonging to the C vs A dataset (cell line comparison) while the other 6 genes were from the F vs E dataset (xenograft comparison). Moving forward, these 6 genes (BMP7, CREB3L1, IGFBP2, MUC4, PRKAR2B, and ZNF662) were analyzed *in vitro*

by IHC and RT-qPCR analyses to ascertain the transcriptomic and nCounter findings in an experimental HNSCC xenograft model (Figure 7).

3.8 Immunohistochemical and RT-qPCR analyses indicated the putative role of MK2-regulated candidate genes in HNSCC pathogenesis

IHC and RT-qPCR were performed to probe the role of the 6 candidate genes in HNSCC pathogenesis and further accentuate the consonance among the transcriptomic and nCounter data analyses. Sections from the xenograft tumor tissues were analyzed using IHC to evaluate the protein expression pattern of the 6 candidate genes (BMP7, CREB3L1, IGFBP2, MUC4, PRKAR2B, and ZNF662) (Figure 7a). The results revealed that xenograft tumor sections with an unregulated expression of these genes have cellular pleomorphism, mitotic figures, and formation of nests of tumor cells, thus, clearly indicating the aggressiveness of HNSCC neoplasms. The results obtained from the IHC analysis largely strengthened the findings of the transcriptomic and nCounter analyses. Out of the 6 candidate genes, *in situ* protein expression levels of MK2-regulated candidate genes IGFBP2, MUC4, and PRKAR2B were found to be upregulated in the tumor xenografts created using CAL27-MK2$_{KD}$ cells as compared to CAL27-MK2$_{WT}$ cells and corroborated with the transcriptome and nCounter analyses (Figure 7a). There was no significant change in the protein expression levels of the 3 other analyzed genes BMP7, CREB3L1, and ZNF662 (data not shown).

Additionally, to examine the role of MK2 in governing the transcript stability of these genes, RT-qPCR analysis was performed in MK2-knockdown cells. CAL27 cells were treated with the shRNA complex to generate CAL27-MK2$_{KD}$ cells as previously described [5] and shown in Figure 7b. Post-knockdown, CAL27-MK2$_{KD,}$ and CAL27-MK2$_{WT}$ (scrambled control transfected cells) were treated with Act-D (1 µM) to halt *de novo* transcription. RT-qPCR was carried out post-Act-D treatments at 6 different time points (0, 0.5, 1, 2, 4, and 8 hours) to determine the transcript expression levels and stability. Transcript levels were

compared for each time point between the WT and KD group. The results revealed that the transcript expression of IGFBP2, MUC4, and PRKAR2B exhibited time-dependent transcriptional decay in CAL27-MK2$_{KD}$ cells as compared to CAL27-MK2$_{WT}$ cells (Figure 7c). The IGFBP2 transcript level was 0.99-fold in CAL27-MK2$_{KD}$ cells which were equivalent to that in CAL27-MK2$_{WT}$ cells (t=0), while the PRKAR2B transcript level was 1.2-fold higher in CAL27-MK2$_{KD}$ cells as compared to CAL27-MK2$_{WT}$ cells (t=0). The expression levels of these genes were stabilized for 1 hour for IGFBP2 and 2 hours for PRKAR2B post-Act-D treatment but gradually showed a significant reduction to less than half the levels (t=4 and t=8) in CAL27-MK2$_{KD}$ cells compared to CAL27-MK2$_{WT}$ cells (Figure 7c). This timeframe of stability may provide sufficient opportunity for the transcript to be expressed and upregulated at the protein level, which was observed in the IHC analysis of the tumor sections (Figure 7c). This suggested that the regulation could be at the transcript level and not at the protein level. However, the MUC4 transcript level was 16-fold lower in CAL27-MK2$_{KD}$ cells as compared to CAL27-MK2$_{WT}$ cells (t=0) but remained stable until 1 hour (t=1) post-Act-D treatment and decreased significantly (>50%) afterward (t=4) (Figure 7c). Taken together, the transcripts of all the 3 genes were degraded in MK2-knockdown cells after maintaining stable transcript levels for a few hours. This finding indicates a strong association of these genes with the expression profile of MK2 in the cells. Conclusively, the results suggested that the expression levels of IGFBP2, MUC4, and PRKAR2B are strongly affected by MK2 expression in HNSCC cells and tumors.

4. Discussion

To improve the understanding of convoluted biology and leverage the outcomes to optimize the management of HNSCC, there have been many efforts to characterize its pathology at the transcript level. Methodological breakthroughs in the recent past have revolutionized the area of transcriptome profiling by providing a link between molecular mechanisms and cellular

phenotypes [23, 49]. In recent times, a comprehensive landscape of genomic and transcriptomic alterations in squamous tumors including HNSCC has emerged by way of the TCGA network [17, 18]. However, cellular models that can comprehensively characterize metastatic HNSCC are still lacking, hence, translationally relevant transcriptome profiling underlying the basis of HNSCC metastasis will prove to be a powerful tool for future preclinical research endeavors [50, 51]. help many established methods help in the detection of DEGs for both microarray-based approaches and RNA-seq [52, 53]. A typical transcriptome profiling result is generally a never-ending list comprising thousands of DEGs, hence, it has always been very difficult to interpret this data without additional filtering *via* functional annotations. A large variety of methods are available for the analysis of DEGs and for obtaining a critical understanding of the pathways, gene regulatory, and co-expression networks involved [54, 55]. In the present study, we undertook the challenge of thoroughly dissecting the huge complexity and large heterogeneity in HNSCC to discern novel biomarkers and potential therapeutic targets.

Keeping in mind the critical findings from previous studies, we performed transcriptome profiling of both the *in vitro* cell line as well as *in vivo* xenograft tumor samples that resulted in thousands of DEGs. These genes were segregated based on their clustering in various biological processes (Table ST2, ST4, and ST6). In line with the primary goal, the processes were filtered based on relevance in cancer leading us to 5 overlapping DEGs in the cell line datasets (A-D), viz. DAP3, EHBP, IP6K2, RUNX1, and SLF2, as listed in Table ST3. EHBP is encoded by the EHBP1 gene, and this protein has been shown to portray a role in actin reorganization and endocytic trafficking [56]. Polymorphism in this gene at the single nucleotide level has been reported to cause prostate cancer [57]. SLF2 is a DNA damage response pathway gene that functions by regulating genomic stability by post-replication repair of damaged DNA [58]. DAP3 has been shown to mediate interferon (IFN)-γ induced cell death in addition to its role in organelle biogenesis as well as

maintenance and mitochondrial translation [59, 60]. DAP3 has been characterized by its pro-apoptotic function as a prognostic factor in gastric cancer and found to be associated with cancer progression [61]. The protein encoded by the IP6K2 gene has been shown to affect growth suppression and apoptotic action of IFN-β in the physiologic regulation of apoptosis in ovarian cancers with its deletion leading to HNSCC predisposition [62]. Lastly, the protein encoded by RUNX1 has been shown to be involved in the activation of EMT *via* the Wnt/β-catenin pathway and the promotion of metastasis in colon cancer [63]. Further, it has been reported that RUNX1 depletion in human HNSCC cells causes growth arrest [64]. Collectively, it is quite evident that all these MK2-regulated genes are playing a vital role in tumor pathogenesis, hence showing consistency with our previous finding of their involvement in HNSCC pathogenesis.

Similarly, a gene regulatory network was generated that depicted a detailed overview of the various inter-connections and the significantly enriched biological processes affected by the DEGs in the 14 cancer-specific biological processes in the transcriptome profiling of the *in vivo* heterotopic HNSCC xenograft dataset (F vs E comparison). TRAF2 has been reported to have a role in the activation of the NF-kappa-B and JNK pathways [34]. EPB41L1 has been shown to have a high prognostic significance and is involved in cell adhesion and migration [34 changed]. FOXO3 is a transcriptional activator known to regulate apoptosis and autophagy in various tumors [36]. H2AFY has been shown to be associated with lipid metabolism and poor prognosis in liver cancer [37]. YAP1 is an important candidate gene of the hippo signaling and has shown to be involved in EMT, immune suppression, and radiation resistance [38]. DIDO1 is a putative transcription factor and has been reported to have weak pro-apoptotic activities [39] (Figure 3b). In lieu of the above arguments and considering the role of the MK2-regulated candidate genes in the experimental analysis, their further exploration as candidates for the development of novel biomarkers and utilization as potential therapeutic targets in HNSCC management is warranted.

Additionally, gene regulatory networks in transcriptome profiling provided information on the various biological processes regulated by these candidate genes. This study supplied a wealth of information that can be further explored to study the pathogenesis of HNSCC in detail, especially in the background of MK2-knockdown and a varied tumor microenvironment (normoxia/hypoxia). Figure 4a is the representation of a gene regulatory network depicting the role of MK2 in the regulation of mRNA stability in the various datasets analyzed and clearly demonstrates that MK2 regulates transcript stability *via* RBP-mediated regulation with HuR (ELAVL1) and TTP (ZFP36) playing integral roles. Similarly, Figure 4b portrays the regulatory network that represents the MAPK signaling cluster of the selected MK2 pathway genes (AUF1, CEBPδ, CUGBP1, HuR, MK2, MKP-1, p27, p38, TNF-α, TTP, and VEGF) in the transcriptome profiling data of the *in vitro* HNSCC cell line dataset (B vs A, normoxic microenvironment) indicated TNF-α and VEGF downregulation. Interestingly, the transcriptomic profiling results are in complete consonance with our recently published findings and hence succeed in potentiating and validating the hypothesis that MK2-knockdown destabilized TNF-α and VEGF in normoxia *via* RBP-mediated interactions [5, 65, 66, 67, 68, 69, 70, 71, 72].

Transcriptome analysis techniques are commonly utilized in endeavors to decipher various molecular mechanisms of tumorigenesis and to fetch out novel prognostic and therapeutic markers [22, 23, 73]. In this study, we aimed to assess the MK2-regulated candidate genes playing prominent roles in HNSCC pathogenesis. Using the 3'-UTR-based filtering criterion detailed before, 34 genes in the *in vitro* A-D datasets and 48 genes in the xenograft dataset (listed in Table ST7 and ST8) were identified. Further validation using the nCounter gene expression assay system enabled the digital quantification and single-molecule imaging of multiple target RNA molecules using multicolor molecular barcodes (Figure S4 and S9). This system provides discrete and accurate counts of RNA transcripts at a high level of sensitivity and precision [32]. The gene expression assays are independent of any

639 enzymatic reactions or amplification protocols and have no reliance on the degree of
640 fluorescence intensity to determine target abundance. As a result of these characteristics, and
641 the highly automated nature of barcoded sample processing, these assays result in highly
642 accurate and reproducible outcomes. On average, approximately 52% matching score of
643 transcriptome profiling data was obtained with nCounter gene expression assay-based
644 validation which is considered a good percentage match considering the high-throughput
645 nature of the analysis and the various datasets analyzed. Filtering of the DEGs in the matched
646 data revealed a list of 12 genes (6 upregulated and 6 downregulated in the various analyzed
647 datasets) that were common in the comprehensive nCounter system-based validation of
648 transcriptomic profiling (Table 4). Intriguingly, these genes portray crucial roles in processes
649 such as apoptosis (CLK2, MELK, MUC4), cell cycle regulation (CLK2, MELK), and
650 transcription regulation (BRD2, H2AFY, SAMD4B, ZNF662).

651 Six candidate genes (BMP7, CREB3L1, IGFBP2, MUC4, PRKAR2B, and ZNF662)
652 showed statistically significant up/downregulation in the xenograft dataset. Insulin-like
653 Growth Factor Binding Protein 2 (IGFBP2) has been shown to be a growth promoter gene in
654 several tumors and is considered a central hub of the oncogenic signaling network governing
655 transcriptional regulation and promoting epithelial to mesenchymal transition, invasion,
656 angiogenesis, and metastasis [74] Recently, IGFBP2 has been reported to be a crucial
657 modulator of metastasis in oral cancer as well [75]. Mucin 4 (MUC4) serves as a major
658 constituent of mucus secreted by epithelial cells and found overexpressed in a variety of
659 cancers such as papillary thyroid carcinomas. It is known for promoting tumor growth,
660 proliferation, and migration [76] [77]. Recent insights have been made into the transcriptional
661 regulation of protein kinase cAMP-dependent type II regulatory subunit beta (PRKAR2B) by
662 miRNAs and X-box binding protein 1 leading to a better understanding of PRKAR2B-driven
663 prostate cancer progression [78]. PRKAR2B has been reported to be involved in the
664 activation of Wnt/β□catenin along with triggering epithelial to mesenchymal transition

665 leading to metastasis in tumors [79]. Consistent with our findings, these genes have been
666 suggested to be prognostic indicators and therapeutic targets in various cancers including
667 HNSCC [74, 75, 76, 77, 78, 79, 80, 81, 82].

668 The protein expression pattern of the 6 candidate genes was further analyzed in tumor
669 sections from xenografted animals. IHC analysis revealed that IGFBP2, MUC4, and
670 PRKAR2B were upregulated and prominently expressed in the cytoplasm and stroma of the
671 tumors generated using CAL27-$MK2_{KD}$ cells (Figure 7a). The expression levels of the other 3
672 genes were not significantly different among the samples. The IHC results were in
673 consonance with the sequencing data, hence, confirming that these genes display differential
674 expression patterns between CAL27-MK_{WT} and CAL27-$MK2_{KD}$ sections. These genes are
675 widely considered imperative to processes such as cell cycle progression, apoptosis, and
676 transcriptional regulation. Various studies have reported their role as central hubs for cellular
677 signaling during oncogenesis and modulating key cellular processes such as apoptosis, cell
678 cycle progression, epithelial-mesenchymal transition, and metastasis [75, 76, 77, 78, 79].
679 Additionally, fewer studies have also reported the contrasting role of these genes in
680 oncogenesis, which is influenced by various factors such as mutation and effects of other
681 genes on the regulation of gene or protein expression of these three genes [83, 84].

682 Furthermore, RT-qPCR analysis was performed to quantify of transcript expression
683 and behavior of these genes *in vitro* under MK_{WT} and $MK2_{KD}$ conditions. CAL27-$MK2_{KD}$
684 cells were treated with Act-D for different time points and mRNA transcript levels of
685 IGFBP2, MUC4, and PRKAR2B were evaluated using transcript expression and stability
686 analysis through RT-qPCR. It was observed that the stability of IGFBP2, PRKAR2B, and
687 MUC4 transcripts decreased temporally in CAL27-$MK2_{KD}$ cells as compared to the CAL27-
688 $MK2_{WT}$ cells. At t=0, the transcript level of IGFBP2 was at the basal level, MUC4 was
689 downregulated while PRKAR2B was upregulated in CAL27-$MK2_{KD}$ cells post-Act-D
690 treatment. Furthermore, this decay increased significantly at t=1 for IGFBP2 and MUC4 and

691 at t=2 for PRKAR2B (Figure 7c). The initial stability of transcripts could account for the
692 upregulated protein expression observed in tumor sections of CAL27-MK2$_{KD}$ xenografted
693 mice as assessed by IHC (Figure 7a). This finding also indicates a strong dependence of
694 IGFBP2, MUC4, and PRKAR2B2 on MK2-mediated regulation *via* RBP-
695 activation/deactivation mechanism. Since these genes have previously been reported to be
696 differentially expressed in tumor conditions, the present study substantiated the hypothesis
697 suggesting the central role of MK2 in this molecular crosstalk. Additionally, these genes have
698 been shown to be involved in a multitude of cellular processes such as the cell cycle,
699 apoptosis, transcription, invasion, and metastasis. The contrasting gene and protein
700 expression levels can be attributed to their regulation either at the transcriptional level or *via*
701 post-translational modifications. This specific scientific question strongly warrants attention
702 and future studies to delve deeper into the role of MK2-mediated activation and deactivation
703 of RBPs that are involved in the transcript stability of these genes. Overall, the results
704 obtained from IHC, and transcript stability analysis indicated the crucial role of MK2 in the
705 modulation of the expression pattern of these genes in HNSCC tumors and cells. Finally,
706 these findings clearly potentiate the importance of these MK2-regulated candidate genes in
707 HNSCC pathogenesis.

708 Conclusively, the results suggested an observed dependence of these candidate genes
709 on MK2 for their transcription in HNSCC cells and xenograft tumors. It is worth mentioning
710 that all these genes are MK2-regulated and potentially play specific roles in HNSCC
711 pathogenesis and progression. This suggests that they could potentially be used as putative
712 candidates for further investigations regarding the design of molecular markers and
713 therapeutics for HNSCC management. Hence, transcriptomic analysis followed by nCounter
714 assay based primary validation, followed by IHC and transcript stability-based secondary
715 validation has provided valuable findings that can aid in extending these observations in
716 future HNSCC-targeted clinical and therapeutic exploratory research.

5. Conclusion

In conclusion, the present study substantiates the involvement of MK2 as a critically important factor in regulating HNSCC by modulating the transcript stability of downstream genes involved in pathogenesis. The probable mechanism of action is *via* RBP-mediated regulation and these results are in perfect consonance and augmentation with recent findings [5]. Comprehensively, few crucial MK2-regulated putative candidate genes were identified in this study, and their plausible involvement in HNSCC pathogenesis was elucidated, which could have further exploratory value as putative targets in HNSCC treatment and management (Figure 7). This study has made it possible to filter down from thousands of DEGs to a few potential candidate genes using comprehensive transcriptomic and *in vitro* validation approaches. To delve deeper into the clinical insights of these findings highlighting the role of MK2-mediated changes in HNSCC pathogenesis, the role of these 3 potential therapeutic targets warrants further detailed investigations for diagnostic and therapeutic interventions of HNSCC.

6. List of Abbreviations

3′-UTR: 3′-untranslated region

ActD: Actinomycin D

ARE(s): Adenylate-uridylate-rich element(s)

ATCC: American Type Culture Collection

CISBP: Catalog of Inferred Sequence Binding Preferences

Ct: Cycle Threshold

DEG(s): Differentially expressed gene(s)

EHBP1: EH domain binding protein 1

SLF2: SMC5-SMC6 complex localization factor 2

DAP3: Death associated protein 3

742 FC: Fold change

743 FDR: False discovery rate

744 FPKM: Fragments per kilobase of transcript per million mapped

745 GFP: Green fluorescent protein

746 GO: Gene Ontology

747 HKG: House keeping genes

748 HNSCCs: Head and neck squamous cell carcinoma(s)

749 HQ: High quality

750 IAEC: Institutional animal ethics committee

751 IFN: Interferon

752 IGFBP2: Insulin-like growth factor-binding protein 2

753 IP6K2: Inositol hexakisphosphate kinase 2

754 IHC: Immunohistochemistry

755 KD: Knockdown

756 KEGG: Kyoto encyclopedia of genes and genomics

757 MAPK: Mitogen-Activated Protein Kinase

758 MAPKAPK2 or MK2: Mitogen-activated protein kinase-activated protein kinase 2

759 $MK2_{KD}$: MK2-knockdown

760 $MK2_{WT}$: MK2 wild-type

761 MELK: Maternal embryonic leucine zipper kinase

762 MUC4: Mucin 4

763 MKP-1: Mitogen-activated protein kinase phosphatase-1

764 NGS: Next generation sequencing

765 NOD/SCID: Non-obese diabetic/severe combined immunodeficient

766 p27: Cyclin-dependent kinase inhibitor 1B

767 PRKAR2B: Protein kinase CAMP-dependent type II regulatory subunit beta

QC: Quality control

RIN: RNA integrity number

RT-qPCR: Real-time quantitative polymerase chain reaction

RBP(s): RNA-binding protein(s)

RNA-seq: Ribose Nucleic Acid -sequencing

RUNX1: Runt-related transcription factor 1

shRNA: Short hairpin RNA

TCGA: The cancer genome atlas

TNF-α: Tumor necrosis factor-alpha

TTP: Tristetraprolin

VEGF: Vascular endothelial growth factor

WB: Western blotting

WT: Wild type

ZNF662: Zinc finger protein 662

7. Declarations

7.1 Availability of Data and materials

The generated datasets (raw reads) from NovaSeq 6000 have been deposited and are available in the National Centre for Biotechnology Information-Sequence Read Archive (NCBI-SRA) repository (https://www.ncbi.nlm.nih.gov/sra). The SRA BioProject accession numbers for the submitted bio projects are PRJNA646850 and PRJNA646851. High-resolution images will be available on request if needed.

7.2 Competing interest

The authors declare that they have no competing interests.

7.3 Funding

This work was supported by the Council of Scientific and Industrial Research, India (CSIR-IHBT; Project MLP0204). Funder: Council of Scientific and Industrial Research, India; Grant Reference Number: Project MLP0204; Author: Dr. Yogendra S. Padwad.

7.4 Authors' contributions

YSP and SS conceptualized, designed the work, and framed the manuscript. SS and PA performed bench work, experiments, and data analysis. MKS helped with RNA-seq and data analysis, VP performed IHC imaging and analysis, and NVT helped in xenograft model generation. SS, PA, VP, and YSP wrote and edited the manuscript. All the authors read and approved the final version of the manuscript.

7.5 Acknowledgments

The authors would like to thanks to the Director, CSIR-IHBT, Palampur for his consistent encouraging support. SS is immensely thankful to CSIR and PA to DST (DST/INSPIRE Fellowship/2017/IF170140) for providing Ph.D. fellowship and Academy of Scientific and Innovative Research (AcSIR), Ghaziabad, India for Ph.D. registration. The authors would like to thank Bionivid Technology Private Limited, Bengaluru, India for their inputs in transcriptome data analysis. CSIR-IHBT communication number of this manuscript is 4682.

7.6 Additional Files

There are 2 Additional files for this manuscript: Additional File 1 (9 supplementary figures, labeled as Figure S1 – Figure S9) and Additional File 2 (10 supplementary tables, labeled as Figure ST1 – Figure ST10).

Figure Legends:

Figure 1: Schematic pictorial illustration of the analysis and validation workflow used for transcriptomic profiling and represents the key outcomes obtained with the work plan.

Detailed analysis work plan and validation scheme indicating the two distinct sample types used for the experimental analysis and their output in terms of DEGs, significant biologies, important filtered out genes, and their validation. Analysis workflow of the dataset obtained from **a)** RNA-seq of cell line samples. **b)** RNA-Seq of tumor xenograft samples. This section represents the initial filtering of the transcriptome data for the identification of crucial biological processes and genes for all the experimental datasets. Additionally, expression levels and gene networks were checked for two categories of genes, first for the genes that are transcriptionally regulated by MK2 and second, for the genes having their mRNA stability controlled by MK2 through RBP-mediated regulation. Thereafter, MK2-regulated transcripts that harbor RBP specific regions in their 3'-UTRs were identified in all datasets, providing 34 genes in A to D comparisons and 48 in F vs E comparisons which were further analyzed by nCounter gene expression analysis. Finally, **c)** validation workflow of the MK2-regulated transcripts that harbor RBP specific regions in their 3'-UTRs filtered out from cell line and tumor samples, and 7 common DEGs in transcriptomic and nCounter gene expression assay were identified, 6 of them from the F vs E dataset were subjected to IHC validation and filtered 3 leads were subjected to transcript stability evaluation.

Figure 2: a) Workflow of sequencing analysis showing sequential steps and various tools and pipelines employed for transcriptome profiling. **b), c)** A comparative bar diagram representation of the number of (b) DEGs; and (c) Significant biologies/Biological processes, present in various datasets in the transcriptome profiling study**. d)** Pie chart representation of the top five GO terms and pathway summary based on all the DEGs in the various datasets showing approximately 5% of the total DEGs belonging to the pathways involved in cancer progression. **e)** Non-hierarchical heatmap representation depicting the expression profile and variation in average log2 fold change among DEGs in various datasets in the transcriptome profiling study. The color bar represents the expression values with green representing the

lowest (downregulation) and red representing the highest (upregulation) expression levels. The various datasets used for expression profiling are labeled on the top. **f)** Volcano plot representation of the complete transcript list according to their average log2 fold change and p-values for various datasets in the transcriptome profiling study with differential transcripts highlighted in blue. The plot displays DEGs along the dimensions of biological significance (average log2 fold change) and statistical significance (p). Genes with an absolute log2 fold change>2 and a p-value<0.05 were considered as DEGs. **g)** Venn diagram representation created using Venny 2.1.0 showing the 77 common elements in the transcriptome profiling of the *in vitro* HNSCC cell line model (A-D datasets). **h)** Venn diagram representation created using Venny 2.1.0 showing the five common genes in the 77 common elements in the transcriptome profiling of the *in vitro* HNSCC cell line model (A-D datasets). **i)** Venn diagram representation created using Venny 2.1.0 showing the two common genes in the 16 common elements in the transcriptome profiling of the *in vitro* HNSCC cell line model (A-D datasets).

Figure 3: Gene regulatory network depicting a detailed overview of the various interconnections and the significantly enriched biological processes affected by the 5 common genes (DAP3, EHBP1, IP6K2, RUNX1 SLF2). Network represented in 77 common elements in the datasets where MK2 knockdown is present; **a)** B vs A comparison of the transcriptome profiling of the *in vitro* HNSCC cell line model. **b)** Gene regulatory network depicting a detailed overview of the various interconnections and the significantly enriched biological processes affected by the DEGs in 14 cancer-specific biological processes in the transcriptome profiling of the *in vivo* heterotopic HNSCC xenograft dataset (F vs E comparison). The gene nodes are sized according to their p-values and colored according to their average log2 fold change, where red shows upregulation while green shows downregulation; processes are shown in rectangular boxes and colored in blue.

865 **Figure 4: a)** Representation of a gene regulatory network depicting the role of MK2 in the
866 regulation of mRNA stability in the various datasets. The figure clearly demonstrates that
867 MK2 regulates transcript stability *via* RBP-mediated regulation with HuR (ELAVL1) and
868 TTP (ZFP36) playing an integral part. **b), c)** Gene regulatory network showing MAPK
869 signaling cluster of the selected MK2 pathway genes (p38, MK2, AUF1, TTP, CUGBP1,
870 CEBPδ, HuR, MKP-1, p27, TNF-α, and VEGF) in the transcriptome profiling data of the (b)
871 *in vitro* HNSCC cell line dataset (B vs A, normoxic microenvironment) indicating VEGF and
872 TNF-α downregulation. (c) In F vs E comparison, these genes which portray essential roles in
873 the MK2 pathway are playing intrinsic roles in certain cellular pathways that are clustered
874 into 6 major biological processes such as immune response, regulation of mRNA stability,
875 regulations of cytokines, MAPK signaling, cell migration, and signaling pathways. The gene
876 nodes are sized according to their p-values and colored according to their average log2 fold
877 change, where red shows upregulation while green shows downregulation and yellow
878 indicates baseline expression; processes are shown in rectangular boxes and colored in blue.

879 **Figure 5:** 3'-UTR based filtering of cancer-specific biological processes from a cell line (16
880 processes) and xenograft tumor (54 processes) datasets to identify MK2-regulated transcripts
881 that harbor RBP specific regions in their 3'-UTRs. **a)** Schematic representation of the applied
882 workplan. **b)** and **c)** Regulatory network of MK2-regulated genes harboring RBP specific
883 regions in their 3'-UTRs; b) total 34 in the B vs A, D vs C, D vs B and C vs A datasets, and c)
884 total 48 in the F vs E datasets. The gene nodes are sized according to their p-values and
885 colored according to their average log2 fold change, where red shows upregulation while
886 green shows downregulation and yellow indicates baseline expression; processes are shown
887 in rectangular boxes and colored in blue.

888 **Figure 6:** Pie chart representation of the top five gene ontologies and pathway summaries
889 based on all the DEGs in the various analyzed datasets used for the nCounter gene expression

assay for **a)** *in vitro* HNSCC cell line model (A-D datasets) and **b)** *in vivo* heterotopic HNSCC xenograft model (F vs E dataset). **c)** Representative nonhierarchical heatmap representation depicting the expression profile and variation in average log2 FC among the DEGs considering the complete CodeSet of 86 genes post-3'-UTR filtering and **d)** the individual CodeSet of 39 selected genes for the *in vitro* HNSCC cell line model (A-D datasets) and 48 selected genes for the *in vivo* heterotopic HNSCC xenograft dataset post-3'UTR-filtering. The various analyzed datasets used for expression profiling are labeled on the top: *in vitro* HNSCC cell line model (A-D datasets) where Lane 1-KDH is Dataset D (CAL27-MK2$_{KD}$ cells in Hypoxia); Lane 2-NH is Dataset C (CAL27-MK2$_{WT}$ cells in Hypoxia); Lane 5-KDN is Dataset B (CAL27-MK2$_{KD}$ cells in Normoxia); Lane 6-NN is Dataset A (CAL27-MK2$_{WT}$ cells in Normoxia), and *in vivo* heterotopic HNSCC xenograft dataset where Lane 3-KDX is CAL27-MK2$_{KD}$ cells grafted (F dataset) and Lane 4-NX is CAL27-MK2$_{WT}$ cells grafted (E dataset). Distinct clusters of upregulated and downregulated genes are visible in each combination. The color bar represents the expression values with green representing the upregulation and red representing the downregulation expression levels.

Figure 7: a) Representation of the *in-situ* protein expression levels of the three candidate MK2-regulated genes (IGFBP2, MUC4, PRKAR2B) in HNSCC xenografted mice tumor sections by immunohistochemical analysis. Different color bars represent the expression values in terms of mean score, the blue bar represents the expression level in CAL27-MK2$_{WT}$ tissue sections (Dataset E), and the red bar signifies *In-situ* protein expression in CAL27-MK2$_{KD}$ tissue sections (Dataset F). Parametric Welch t-test was used to evaluate the statistical significance using GraphPad Prism 7.0 software, ** denotes $p<0.01$; n=5 field views for IHC analysis. **b)** Western blot depicting MK2 expression in CAL27-MK2$_{KD}$ cells generated post MK2 knockdown using shRNA for transcript stability experiment, here, SC-

Scrambled control; shMix- A combination of an equal quantity of MK2 targeting shRNA complexes 1, 2, 3, and 4; the shMix group was used for transcript stability experiments, and SC was used as a control. **c)** Gene expression patterns of the 3 candidate genes in CAL27-$MK2_{KD}$ cells at different time points post-Act-D treatment to assess the role of MK2 in regulating transcript stability. Data points represent the fold change in the shMix group at a particular time interval as compared to the control group. Linear regression analysis was performed using GraphPad Prism 7.0 software. **d)** Pictorial representation of the MAPK pathway analyzed in this study, the illustration depicts the activation of MK2 and the plausible mode of action in HNSCC pathogenesis. Figure elucidates the final MK2-regulated putative candidate genes in the pathway that were obtained in this study which could be further explored as possible targets for HNSCC management.

References

1. Spataro N, Rodríguez JA, Navarro A, Bosch E. Properties of human disease genes and the role of genes linked to Mendelian disorders in complex disease aetiology. Human Molecular Genetics. 2017 Feb 1;26(3):489–500. https://doi.org/10.1093/hmg/ddw405

2. Lasa M, Mahtani KR, Finch A, Brewer G, Saklatvala J, Clark AR. Regulation of Cyclooxygenase 2 mRNA Stability by the Mitogen-Activated Protein Kinase p38 Signaling Cascade. Molecular and Cellular Biology. 2000 Jun 15;20(12):4265–74. https://doi.org/10.1128/mcb.20.12.4265-4274.2000

3. Venigalla RK, Turner M. RNA-binding proteins as a point of convergence of the PI3K and p38 MAPK pathways. Frontiers in Immunology. 2012;3:398. https://doi.org/10.3389/fimmu.2012.00398

4. Soni S, Anand P, Padwad YS. MAPKAPK2: the master regulator of RNA-binding proteins modulates transcript stability and tumor progression. Journal of Experimental & Clinical Cancer Research. 2019 Mar 8;38(1):121. https://doi.org/10.1186/s13046-019-1115-1

5. Soni S, Saroch MK, Chander B, Tirpude NV, Padwad YS. MAPKAPK2 plays a crucial role in the progression of head and neck squamous cell carcinoma by regulating transcript stability. Journal of Experimental & Clinical Cancer Research. 2019 Apr 25;38(1):175. https://doi.org/10.1186/s13046-019-1167-2

6. Chow LQM. Head and neck cancer. New England Journal of Medicine 2020; 382(1):60–72. https://doi.org/doi:10.1056/NEJMra1715715

7. Siegel RL, Miller KD, Fuchs HE, Jemal A. Cancer statistics, 2021. CA: A Cancer Journal for Clinicians 2021; 71(1):7–33. https://doi.org/10.3322/caac.21654

8. Woolgar JA, Triantafyllou A. Squamous cell carcinoma and precursor lesions: clinical pathology. Periodontology 2000. 2011;57(1):51–72. https://doi.org/10.1111/j.1600-0757.2011.00389.x

9. Martin D, Abba MC, Molinolo AA, Vitale-Cross L, Wang Z, Zaida M, et al. The head and neck cancer cell oncogenome: A platform for the development of precision molecular therapies. Oncotarget. 2014 Nov 4;5(19):8906–23. https://doi.org/10.18632/oncotarget.2417

10. Waes CV, Musbahi O. Genomics and advances towards precision medicine for head and neck squamous cell carcinoma. Laryngoscope Investigative Otolaryngology. 2017;2(5):310–9. https://doi.org/10.1002/lio2.86

11. Denaro N, Russi EG, Adamo V, Merlano MC. State-of-the-Art and Emerging Treatment Options in the Management of Head and Neck Cancer: News from 2013. OCL. 2014;86(4):212–29. https://doi.org/10.1159/000357712

12. Narayanan SP, Singh S, Gupta A, Yadav S, Singh SR, Shukla S. Integrated genomic analyses identify KDM1A's role in cell proliferation via modulating E2F signaling activity and associate with poor clinical outcome in oral cancer. Cancer Letters. 2015 Oct 28;367(2):162–72. https://doi.org/10.1016/j.canlet.2015.07.022

13. Jamali Z, Asl Aminabadi N, Attaran R, Pournagiazar F, Ghertasi Oskouei S, Ahmadpour F. MicroRNAs as prognostic molecular signatures in human head and neck squamous cell carcinoma: A systematic review and meta-analysis. Oral Oncology. 2015 Apr 1;51(4):321–31. https://doi.org/10.1016/j.oraloncology.2015.01.008

14. Weinberg RA. Coming Full Circle—From Endless Complexity to Simplicity and Back Again. Cell. 2014 Mar 27;157(1):267–71. https://doi.org/10.1016/j.cell.2014.03.004

15. Chau NG, Li YY, Jo VY, Rabinowits G, Lorch JH, Tishler RB, et al. Incorporation of Next-Generation Sequencing into Routine Clinical Care to Direct Treatment of Head and Neck Squamous Cell Carcinoma. Clin Cancer Res. 2016 Jun 15;22(12):2939–49. https://doi.org/10.1158/1078-0432.CCR-15-2314

16. Bossi P, Bergamini C, Siano M, Rocca MC, Sponghini AP, Favales F, et al. Functional Genomics Uncover the Biology behind the Responsiveness of Head and Neck Squamous Cell Cancer Patients to Cetuximab. Clin Cancer Res. 2016 Aug 1;22(15):3961–70. https://doi.org/10.1158/1078-0432.CCR-15-2547

17. Lawrence MS, Sougnez C, Lichtenstein L, Cibulskis K, Lander E, Gabriel SB, et al. Comprehensive genomic characterization of head and neck squamous cell carcinomas. Nature. 2015 Jan;517(7536):576–82. https://doi.org/10.1038/nature14129

18. Campbell JD, Yau C, Bowlby R, Liu Y, Brennan K, Fan H, et al. Genomic, Pathway Network, and Immunologic Features Distinguishing Squamous Carcinomas. Cell Reports. 2018 Apr 3;23(1):194-212.e6. https://doi.org/10.1016/j.celrep.2018.03.063

19. Chakraborty A. The inositol pyrophosphate pathway in health and diseases. Biological Reviews. 2018 May;93(2):1203-27. https://doi.org/10.1111/brv.12392

20. Bhatia S, Frangioni JV, Hoffman RM, Iafrate AJ, Polyak K. The challenges posed by cancer heterogeneity. Nat Biotechnol. 2012 Jul;30(7):604–10. https://doi.org/10.1038/nbt.2294

21. Fiore M, Forli S, Manetti F. Targeting Mitogen-Activated Protein Kinase-Activated Protein Kinase 2 (MAPKAPK2, MK2): Medicinal Chemistry Efforts To Lead Small Molecule Inhibitors to Clinical Trials. J Med Chem. 2016 Apr 28;59(8):3609–34. https://doi.org/10.1021/acs.jmedchem.5b01457

22. Fang X-N, Yin M, Li H, Liang C, Xu C, Yang G-W, et al. Comprehensive analysis of competitive endogenous RNAs network associated with head and neck squamous cell carcinoma. Sci Rep. 2018 Jul 12;8(1):10544. https://doi.org/10.1038/s41598-018-28957-y

23. Cieślik M, Chinnaiyan AM. Cancer transcriptome profiling at the juncture of clinical translation. Nat Rev Genet. 2018 Feb;19(2):93–109. https://doi.org/10.1038/nrg.2017.96

24. Swarnkar MK, Kumar P, Dogra V, Kumar S. Prickle morphogenesis in rose is coupled with secondary metabolite accumulation and governed by canonical MBW transcriptional complex. Plant direct. 2021 Jun;5(6):e00325.

25. Patel RK, Jain M. NGS QC Toolkit: A Toolkit for Quality Control of Next Generation Sequencing Data. PLOS ONE. 2012 Feb 1;7(2):e30619. https://doi.org/10.1371/journal.pone.0030619

26. Mortazavi A, Williams BA, McCue K, Schaeffer L, Wold B. Mapping and quantifying mammalian transcriptomes by RNA-Seq. Nature methods. 2008 Jul;5(7):621-8. https://doi.org/10.1038/nmeth.1226

27. Anders, S. and Huber, W., 2010. Differential expression analysis for sequence count data. Nature Precedings, pp.1-1. https://doi.org/10.1186/gb-2010-11-10-r106

28. Huang DW, Sherman BT, Lempicki RA. Bioinformatics enrichment tools: paths toward the comprehensive functional analysis of large gene lists. Nucleic Acids Research. 2009 Jan 1;37(1):1–13. https://doi.org/10.1093/nar/gkn923

29. Huang DW, Sherman BT, Lempicki RA. Systematic and integrative analysis of large gene lists using DAVID bioinformatics resources. Nat Protoc. 2009 Jan;4(1):44–57. https://doi.org/10.1038/nprot.2008.211

30. Dennis G, Sherman BT, Hosack DA, Yang J, Gao W, Lane HC, et al. DAVID: Database for Annotation, Visualization, and Integrated Discovery. Genome Biology. 2003 Aug 14;4(9):R60. https://doi.org/10.1186/gb-2003-4-9-r60

31. Montojo J, Zuberi K, Rodriguez H, Kazi F, Wright G, Donaldson SL, et al. GeneMANIA Cytoscape plugin: fast gene function predictions on the desktop.

Bioinformatics. 2010 Nov 15;26(22):2927–8. https://doi.org/10.1093/bioinformatics/btq562

32. Brumbaugh CD, Kim HJ, Giovacchini M, Pourmand N. NanoStriDE: normalization and differential expression analysis of NanoString nCounter data. BMC Bioinformatics. 2011 Dec 16;12(1):479. https://doi.org/10.1186/1471-2105-12-479

33. Wazir U, Orakzai MM, Khanzada ZS, Jiang WG, Sharma AK, Kasem A, et al. The role of death-associated protein 3 in apoptosis, anoikis and human cancer. Cancer Cell International. 2015 Apr 10;15(1):39. https://doi.org/10.1186/s12935-015-0187-z

34. Zhang MH, Zhang HH, Du XH, Gao J, Li C, Shi HR, Li SZ. UCHL3 promotes ovarian cancer progression by stabilizing TRAF2 to activate the NF-κB pathway. Oncogene. 2020 Jan;39(2):322-33. https://doi.org/10.1038/s41388-019-0987-z

35. Liang T, Sang S, Shao Q, Chen C, Deng Z, Wang T, Kang Q. Abnormal expression and prognostic significance of EPB41L1 in kidney renal clear cell carcinoma based on data mining. Cancer cell international. 2020 Dec;20(1):1-4. https://doi.org/10.1186/s12935-020-01449-8

36. Liu Y, Ao X, Ding W, Ponnusamy M, Wu W, Hao X, Yu W, Wang Y, Li P, Wang J. Critical role of FOXO3a in carcinogenesis. Molecular cancer. 2018 Dec;17(1):1-2. https://doi.org/10.1186/s12943-018-0856-3

37. Ma X, Ding Y, Zeng L. The diagnostic and prognostic value of H2AFY in hepatocellular carcinoma. BMC Cancer. 2021 Apr 15;21(1):418. https://doi.org/10.1186/s12885-021-08161-4

38. Li F, Xu Y, Liu B, Singh PK, Zhao W, Jin J, et al. YAP1-Mediated CDK6 Activation Confers Radiation Resistance in Esophageal Cancer – Rationale for the Combination

of YAP1 and CDK4/6 Inhibitors in Esophageal Cancer. Clin Cancer Res. 2019 Apr 1;25(7):2264–77. https://doi.org/10.1158/1078-0432.CCR-18-1029

39. Li J, Wang AS, Wang S, Wang CY, Xue S, Li WY, Ma TT, Shan YX. Death-inducer obliterator 1 (DIDO1) silencing suppresses the growth of bladder cancer cells through decreasing SAPK/JNK signaling cascades. Neoplasma. 2020 Jan 1;67(5):1074-84. https://doi.org/10.4149/neo_2020_191115N01171

40. Winzen R, Kracht M, Ritter B, Wilhelm A, Chen CY, Shyu AB, Müller M, Gaestel M, Resch K, Holtmann H. The p38 MAP kinase pathway signals for cytokine-induced mRNA stabilization via MAP kinase-activated protein kinase 2 and an AU-rich region-targeted mechanism. The EMBO journal. 1999 Sep 15;18(18):4969-80. https://doi.org/10.1093/emboj/18.18.4969

41. Krismer K, Bird MA, Varmeh S, Handly ED, Gattinger A, Bernwinkler T, Anderson DA, Heinzel A, Joughin BA, Kong YW, Cannell IG. Transite: A computational motif-based analysis platform that identifies RNA-binding proteins modulating changes in gene expression. Cell reports. 2020 Aug 25;32(8):108064. https://doi.org/10.1016/j.celrep.2020.108064

42. Vejnar, C.E., Messih, M.A., Takacs, C.M., Yartseva, V., Oikonomou, P., Christiano, R., Stoeckius, M., Lau, S., Lee, M.T., Beaudoin, J.D. and Musaev, D., 2019. Genome wide analysis of 3′ UTR sequence elements and proteins regulating mRNA stability during maternal-to-zygotic transition in zebrafish. Genome research, 29(7), pp.1100-1114. https://doi.org/10.1101/gr.245159.118

43. Plass M, Rasmussen SH, Krogh A. Highly accessible AU-rich regions in 3'untranslated regions are hotspots for binding of regulatory factors. PLoS

computational biology. 2017 Apr 14;13(4):e1005460. https://doi.org/10.1007/978-1-0716-1851-6_3

44. Aken BL, Ayling S, Barrell D, Clarke L, Curwen V, Fairley S, et al. The Ensembl gene annotation system. Database [Internet]. 2016 Jan 1 [cited 2021 Aug 25];2016(baw093). Available from: https://doi.org/10.1093/database/baw093

45. Ray D, Kazan H, Cook KB, Weirauch MT, Najafabadi HS, Li X, Gueroussov S, Albu M, Zheng H, Yang A, Na H. A compendium of RNA-binding motifs for decoding gene regulation. Nature. 2013 Jul;499(7457):172-7. https://doi.org/10.1038/nature12311

46. Paz, I., Argoetti, A., Cohen, N., Even, N. and Mandel-Gutfreund, Y., 2022. RBPmap: A Tool for Mapping and Predicting the Binding Sites of RNA-Binding Proteins Considering the Motif Environment. In Post-Transcriptional Gene Regulation (pp. 53-65). Humana, New York, NY. https://doi.org/10.1007/978-1-0716-1851-6_3

47. Lallemant B, Evrard A, Combescure C, Chapuis H, Chambon G, Raynal C, et al. Reference gene selection for head and neck squamous cell carcinoma gene expression studies. BMC Molecular Biology. 2009 Aug 3;10(1):78. https://doi.org/10.1186/1471-2199-10-78

48. Palve V, Pareek M, Krishnan NM, Siddappa G, Suresh A, Kuriakose MA, et al. A minimal set of internal control genes for gene expression studies in head and neck squamous cell carcinoma. PeerJ. 2018 Aug 14;6:e5207. https://doi.org/10.7717/peerj.5207

49. Cheng H, Yang X, Si H, Saleh AD, Xiao W, Coupar J, et al. Genomic and Transcriptomic Characterization Links Cell Lines with Aggressive Head and Neck

1096 Cancers. Cell Reports. 2018 Oct 30;25(5):1332-1345.e5.
1097 https://doi.org/10.1016/j.celrep.2018.10.007

1098 50. Byron SA, Van Keuren-Jensen KR, Engelthaler DM, Carpten JD, Craig DW.
1099 Translating RNA sequencing into clinical diagnostics: opportunities and challenges.
1100 Nat Rev Genet. 2016 May;17(5):257–71. https://doi.org/10.1038/nrg.2016.10

1101 51. Nisa L, Barras D, Medová M, Aebersold DM, Medo M, Poliaková M, et al.
1102 Comprehensive Genomic Profiling of Patient-matched Head and Neck Cancer Cells:
1103 A Preclinical Pipeline for Metastatic and Recurrent Disease. Mol Cancer Res. 2018
1104 Dec 1;16(12):1912–26. https://doi.org/10.1158/1541-7786.MCR-18-0056

1105 52. Scholtens D, von Heydebreck A. Analysis of Differential Gene Expression Studies.
1106 In: Gentleman R, Carey VJ, Huber W, Irizarry RA, Dudoit S, editors. Bioinformatics
1107 and Computational Biology Solutions Using R and Bioconductor [Internet]. New
1108 York, NY: Springer; 2005 [cited 2021 Aug 26]. p. 229–48. (Statistics for Biology and
1109 Health). Available from: https://doi.org/10.1007/0-387-29362-0_14

1110 53. Love MI, Huber W, Anders S. Moderated estimation of fold change and dispersion
1111 for RNA-seq data with DESeq2. Genome Biology. 2014 Dec 5;15(12):550.
1112 https://doi.org/10.1186/s13059-014-0550-8

1113 54. Ackermann M, Strimmer K. A general modular framework for gene set enrichment
1114 analysis. BMC Bioinformatics. 2009 Feb 3;10(1):47. https://doi.org/10.1186/1471-
1115 2105-10-47

1116 55. Mitrea C, Taghavi Z, Bokanizad B, Hanoudi S, Tagett R, Donato M, et al. Methods
1117 and approaches in the topology-based analysis of biological pathways. Frontiers in
1118 Physiology. 2013;4:278. https://doi.org/10.3389/fphys.2013.00278

56. Guilherme A, Soriano NA, Bose S, Holik J, Bose A, Pomerleau DP, et al. EHD2 and the Novel EH Domain Binding Protein EHBP1 Couple Endocytosis to the Actin Cytoskeleton*. Journal of Biological Chemistry. 2004 Mar 12;279(11):10593–605. https://doi.org/10.1074/jbc.M307702200

57. Sun J, Kader AK, Hsu F-C, Kim S-T, Zhu Y, Turner AR, et al. Inherited genetic markers discovered to date are able to identify a significant number of men at considerably elevated risk for prostate cancer. The Prostate. 2011;71(4):421–30. https://doi.org/10.1002/pros.21256

58. Han X, Wang Z, Zhang L, Shen Y, Tan Q, Sun Y, et al. SLF1 polymorphism predicts response to oxaliplatin-based adjuvant chemotherapy in patients with colon cancer. Am J Cancer Res. 2021 Apr 15;11(4):1522–39. https://doi.org/10.1126/science.1253671

59. Kissil JL, Deiss LP, Bayewitch M, Raveh T, Khaspekov G, Kimchi A. Isolation of DAP3, a Novel Mediator of Interferon-γ-induced Cell Death (*). Journal of Biological Chemistry. 1995 Nov 17;270(46):27932–6. https://doi.org/10.1074/jbc.270.46.27932

60. Tang T, Zheng B, Chen S, Murphy AN, Kudlicka K, Zhou H, et al. hNOA1 Interacts with Complex I and DAP3 and Regulates Mitochondrial Respiration and Apoptosis*. Journal of Biological Chemistry. 2009 Feb 20;284(8):5414–24. https://doi.org/10.1074/jbc.M807797200

61. Han J, An O, Hong H, Chan THM, Song Y, Shen H, et al. Suppression of adenosine-to-inosine (A-to-I) RNA editome by death associated protein 3 (DAP3) promotes cancer progression. Science Advances. 2020 Jun 1;6(25):eaba5136. https://doi.org/10.1038/bjc.2013.712

62. Morrison BH, Bauer JA, Hu J, Grane RW, Ozdemir AM, Chawla-Sarkar M, et al. Inositol hexakisphosphate kinase 2 sensitizes ovarian carcinoma cells to multiple cancer therapeutics. Oncogene. 2002 Mar;21(12):1882–9. https://doi.org/10.1038/sj.onc.1205265

63. Li Q, Lai Q, He C, Fang Y, Yan Q, Zhang Y, et al. RUNX1 promotes tumour metastasis by activating the Wnt/β-catenin signalling pathway and EMT in colorectal cancer. J Exp Clin Cancer Res. 2019 Aug 1;38(1):334. https://doi.org/10.1182/blood-2016-10-687830

64. Taniuchi I, Osato M, Ito Y. Runx1: no longer just for leukemia. The EMBO journal. 2012 Nov 5;31(21):4098-9. https://doi.org/10.1038/emboj.2012.282

65. Guo J, Qu H, Chen Y, Xia J. The role of RNA-binding protein tristetraprolin in cancer and immunity. Med Oncol. 2017 Dec;34(12):196. https://doi.org/10.1007/s12032-017-1055-6

66. Balamurugan K, Mendoza-Villanueva D, Sharan S, Summers GH, Dobrolecki LE, Lewis MT, Sterneck E. C/EBPδ links IL-6 and HIF-1 signaling to promote breast cancer stem cell-associated phenotypes. Oncogene. 2019 May;38(20):3765-80. https://doi.org/10.1038/s41388-018-0516-5

67. Zhang Y, Yang L, Ling C, Heng W. HuR facilitates cancer stemness of lung cancer cells via regulating miR-873/CDK3 and miR-125a-3p/CDK3 axis. Biotechnol Lett. 2018 Apr 1;40(4):623–31. https://doi.org/10.1007/s10529-018-2512-9

68. Hammad A, Zheng Z-H, Namani A, Elshaer M, Wang XJ, Tang X. Transcriptome analysis of potential candidate genes and molecular pathways in colitis-associated

colorectal cancer of Mkp-1-deficient mice. BMC Cancer. 2021 May 25;21(1):607. https://doi.org/10.1186/s12885-021-08200-0

69. Razavipour SF, Harikumar KB, Slingerland JM. p27 as a Transcriptional Regulator: New Roles in Development and Cancer. Cancer Res. 2020 Sep 1;80(17):3451–8. https://doi.org/10.1158/0008-5472.CAN-19-3663

70. Montfort A, Dufau C, Colacios C, Andrieu-Abadie N, Levade T, Filleron T, et al. Anti-TNF, a magic bullet in cancer immunotherapy? j immunotherapy cancer. 2019 Nov 14;7(1):303. https://doi.org/10.1186/s40425-019-0802-y

71. Siemert J, Wald T, Kolb M, Pettinella I, Böhm U, Pirlich M, et al. Pre-Therapeutic VEGF Level in Plasma Is a Prognostic Bio-Marker in Head and Neck Squamous Cell Carcinoma (HNSCC). Cancers. 2021 Jan;13(15):3781. https://doi.org/10.3390/cancers13153781

72. Bergers G, Hanahan D. Modes of resistance to anti-angiogenic therapy. Nat Rev Cancer. 2008 Aug;8(8):592–603. https://doi.org/10.1038/nrc2442

73. Trapnell C, Williams BA, Pertea G, Mortazavi A, Kwan G, van Baren MJ, et al. Transcript assembly and quantification by RNA-Seq reveals unannotated transcripts and isoform switching during cell differentiation. Nat Biotechnol. 2010 May;28(5):511–5. https://doi.org/10.1038/nbt.1621

74. Lindström MS. Expanding the scope of candidate prognostic marker IGFBP2 in glioblastoma. Bioscience reports. 2019 Jul;39(7):BSR20190770. https://doi.org/10.1042/BSR20190770

75. Tsai Y-F, Chou H-C, Liou M-H, Liao E-C, Cheng C-T, Chang S-J, et al. Role of IGFBP-2 in oral cancer metastasis. Biochimica et Biophysica Acta (BBA) - Molecular

1187 Basis of Disease. 2021 Jul 1;1867(7):166143.
1188 https://doi.org/10.1016/j.bbadis.2021.166143

1189 76. Reynolds IS, Fichtner M, McNamara DA, Kay EW, Prehn JH, Burke JP. Mucin
1190 glycoproteins block apoptosis; promote invasion, proliferation, and migration; and
1191 cause chemoresistance through diverse pathways in epithelial cancers. Cancer and
1192 Metastasis Reviews. 2019 Jun;38(1):237-57. https://doi.org/10.1007/s10555-019-
1193 09781-w

1194 77. Xia P, Choi AH, Deng Z, Yang Y, Zhao J, Wang Y, et al. Cell membrane-anchored
1195 MUC4 promotes tumorigenicity in epithelial carcinomas. Oncotarget. 2016 Nov
1196 4;8(8):14147–57. https://doi.org/10.18632/oncotarget.13122

1197 78. Xia L, Han Q, Chi C, Zhu Y, Pan J, Dong B, et al. Transcriptional regulation of
1198 PRKAR2B by miR-200b-3p/200c-3p and XBP1 in human prostate cancer.
1199 Biomedicine & Pharmacotherapy. 2020 Apr 1;124:109863.
1200 https://doi.org/10.1016/j.biopha.2020.109863

1201 79. Sha J, Han Q, Chi C, Zhu Y, Pan J, Dong B, Huang Y, Xia W, Xue W. PRKAR2B
1202 promotes prostate cancer metastasis by activating Wnt/β□catenin and inducing
1203 epithelial□mesenchymal transition. Journal of cellular biochemistry. 2018
1204 Sep;119(9):7319-27. https://doi.org/10.1002/jcb.27030

1205 80. Park J, Lee J, Choi C. Evaluation of drug-targetable genes by defining modes of
1206 abnormality in gene expression. Sci Rep. 2015 Sep 4;5(1):13576.
1207 https://doi.org/10.1038/srep13576

81. Thangaraj K, Ponnusamy L, Natarajan SR, Manoharan R. MELK/MPK38 in cancer: from mechanistic aspects to therapeutic strategies. Drug Discovery Today. 2020 Dec 1;25(12):2161–73. https://doi.org/10.1016/j.drudis.2020.09.029

82. Zhao C, Zou H, Zhang J, Wang J, Liu H. An integrated methylation and gene expression microarray analysis reveals significant prognostic biomarkers in oral squamous cell carcinoma. Oncology Reports. 2018 Nov 1;40(5):2637–47. https://doi.org/10.3892/or.2018.6702

83. Li, T., Forbes, M.E., Fuller, G.N. *et al.* IGFBP2: integrative hub of developmental and oncogenic signaling network. *Oncogene* **39,** 2243–2257 (2020). https://doi.org/10.1038/s41388-020-1154-2

84. Matuschek G, Rudoy M, Peiper M, Gerber PA, Hoff NP, Buhren BA, Flehmig B, Budach W, Knoefel WT, Bojar H, Prisack HB. Do insulin-like growth factor associated proteins qualify as a tumor marker? Results of a prospective study in 163 cancer patients. European journal of medical research. 2011 Dec;16(10):451-6. https://doi.org/10.1186/2047-783X-16-10-451

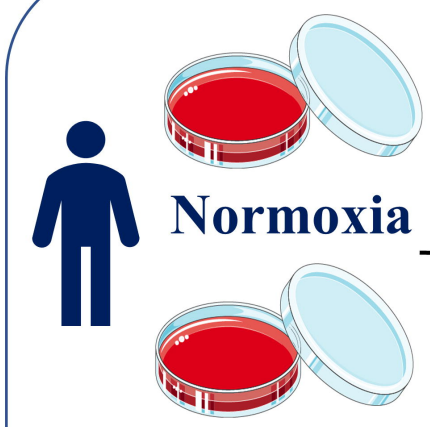

Normoxia

Hypoxia

Subcutaneous injection of CAL27

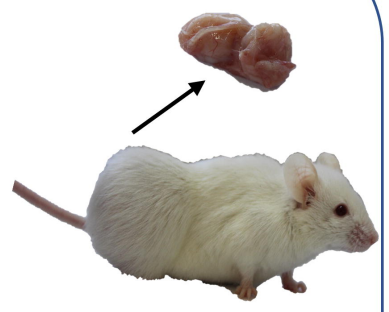

Xenografted tumor

CAL27/MK2wt, CAL27/MK2KD

RNA

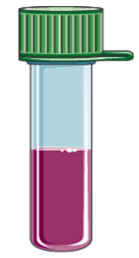

cDNA library

Next generation sequencing (RNASeq)

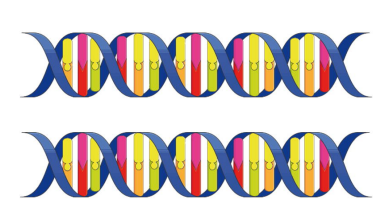

Computational analysis

Secondary validation

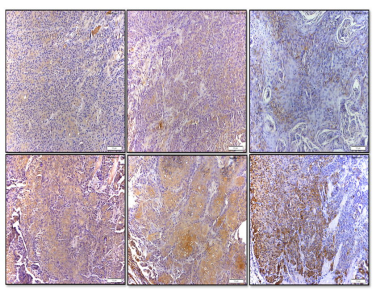

IHC

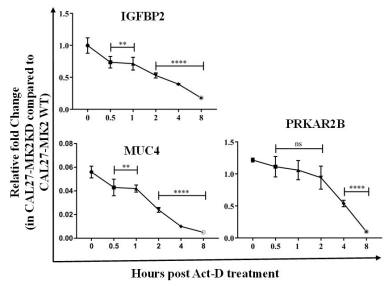

Transcript stability

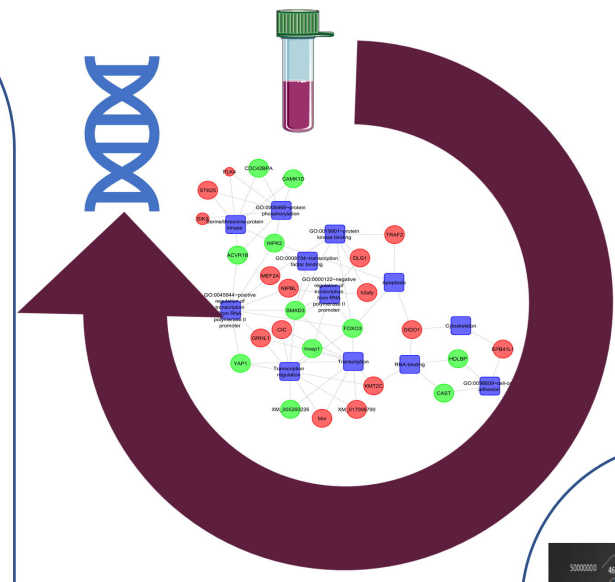

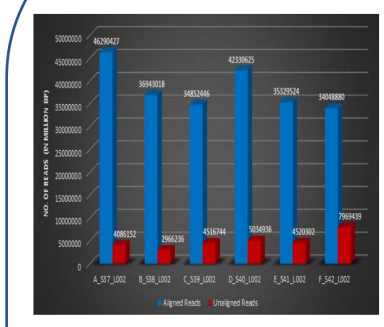

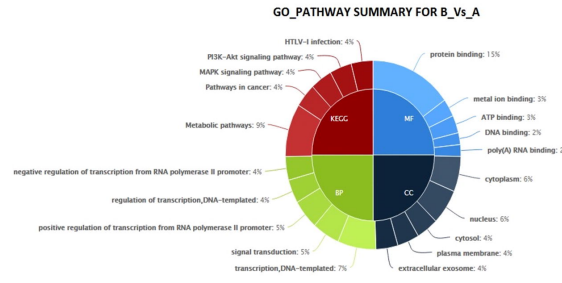

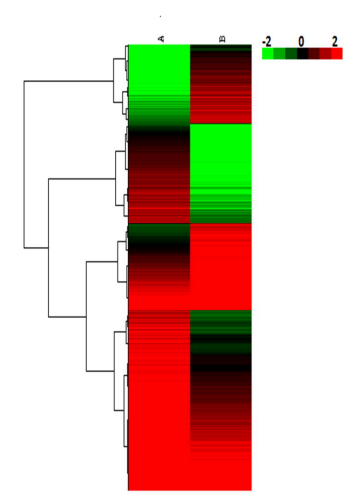

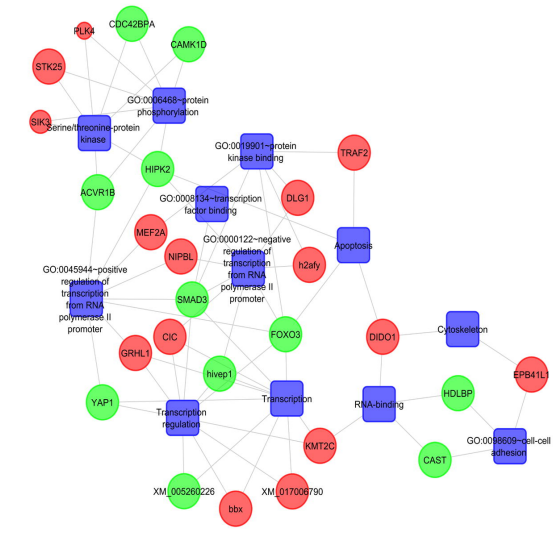

HIGHLY MULTIPLEXED SINGLE MOLECULE COUNTING

NanoString's patented molecular barcodes provide a true digital detection technology capable of highly multiplexed analysis*.

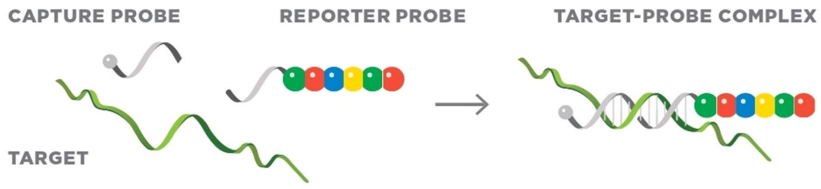

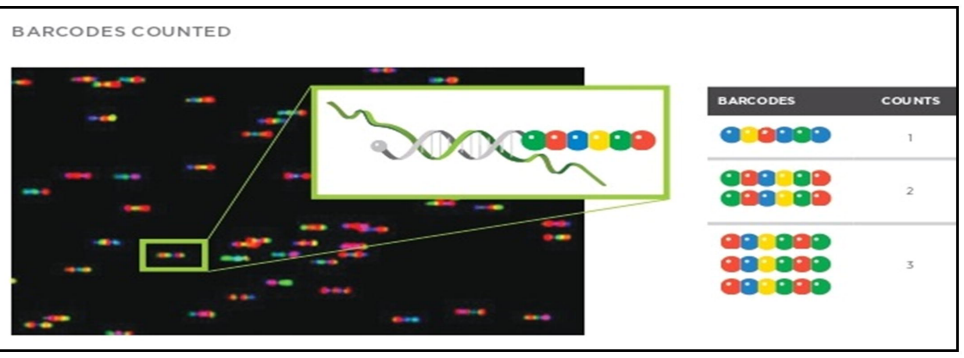

86 Target genes

Absolute transcript quantification by nCounter gene expression assay

Primary validation

RNAseq Dataset: A,B,C,D (Cell Line) and E & F (Xenograft)

Cell Line

a)

5143 DEGs

2195 Significant Biologies

5 Common genes (DAP3, EHBP1, IP6K2, RUNX1 SLF2,)

77 Common biologies between A-D

2 Common genes (DAP3, RUNX1)

16 Cancer specific biologies

Clustering

5 KEGG pathways
- Apoptosis
- Apoptosis and Transcription
- Protein phosphorylation
- Transcriptional Regulation
- Cytoskeleton

KEGG pathway enrichment analysis

Xenograft

b)

408 Significant Biologies

984 DEGs

14 Cancer specific biologies

Key Genes (DIDO1, EPB41L1, FOXO3, H2AFY, TRAF2, YAP1,)

6 MK2-regulated pathways

Selected genes of the MK2 pathway transcriptionally regulated by MK2

(AUF1, CEBPδ, CUGBP1, ELAVL1, HuR, MKP-1, p27, TNF-α, TTP, VEGF, ZFP36)

MK2-regulated transcripts that harbor RBP specific regions in their 3'-UTRs

5 Common genes

34 MK2-regulated Genes

48 MK2-regulated Genes

c)

Validation Protocol

Nanostring n-Counter Gene Expression Assay

7 common DEGs in transcriptomic and nCounter analysis (FC>2 or <-2, p<0.05)
BMP7, CREB3L1, IGFBP2, MELK, MUC4, PRKAR2B, ZNF662

6 selected DEGs BMP7, CREB3L1, IGFBP2, MUC4, PRKAR2B, ZNF662

Immunohistochemistry (IHC)

IGFBP2

MUC4

MK2

PRAKARB2

3 key genes IGFBP2, MUC4, PRKAR2B

Transcript stability

Primary Validation .
Nanostring n-Counter Assay using custom designed molecular barcodes for single molecule imaging

Secondary Validation
Immunohistochemical analysis to detect *in-situ* expression of proteins in xenograft tissue samples

RT-qPCR to check the expression levels of selected genes and their dependence on MK2

a)

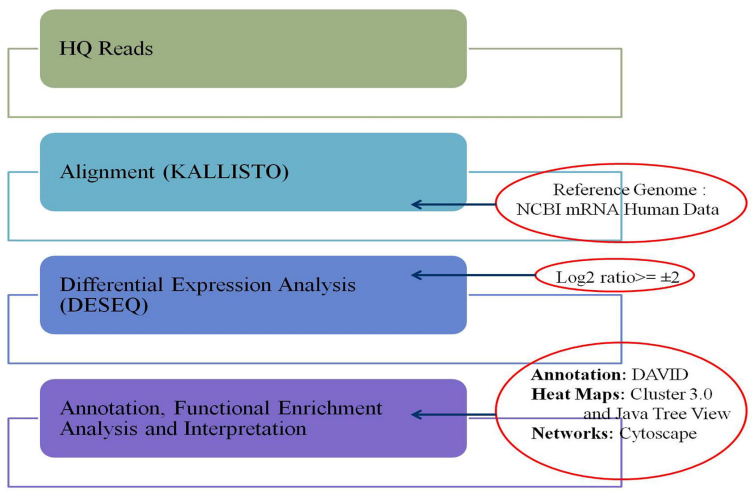

b)

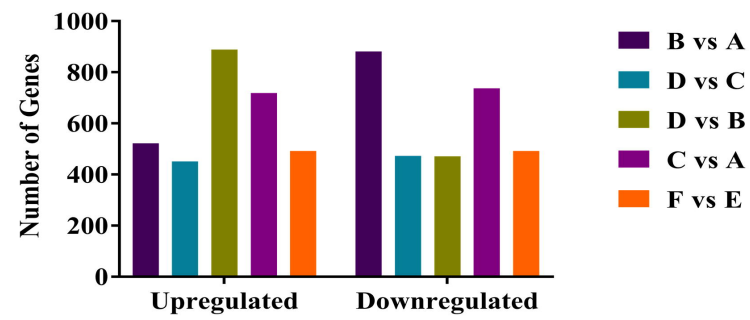

	B vs A	D vs C	D vs B	C vs A	F vs E
Up	522	451	889	719	492
Down	881	473	471	737	492

c)

	B vs A	D vs C	D vs B	C vs A	F vs E
No. of Significant Biologies	643	401	531	620	408

d)

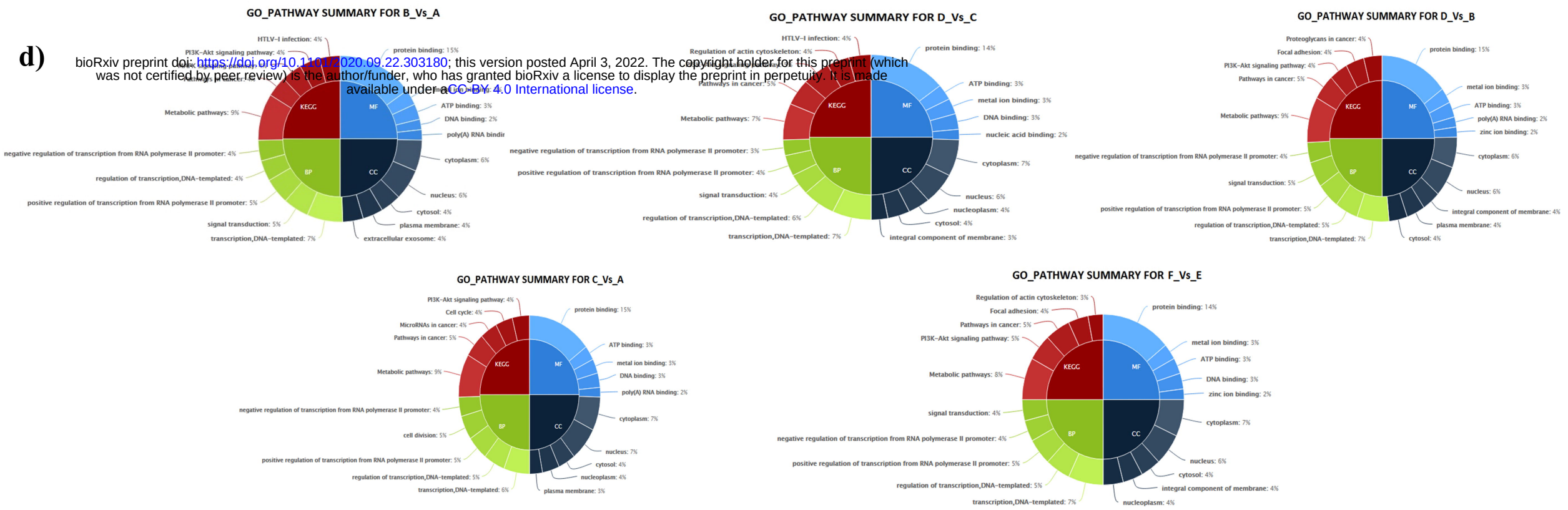

e)

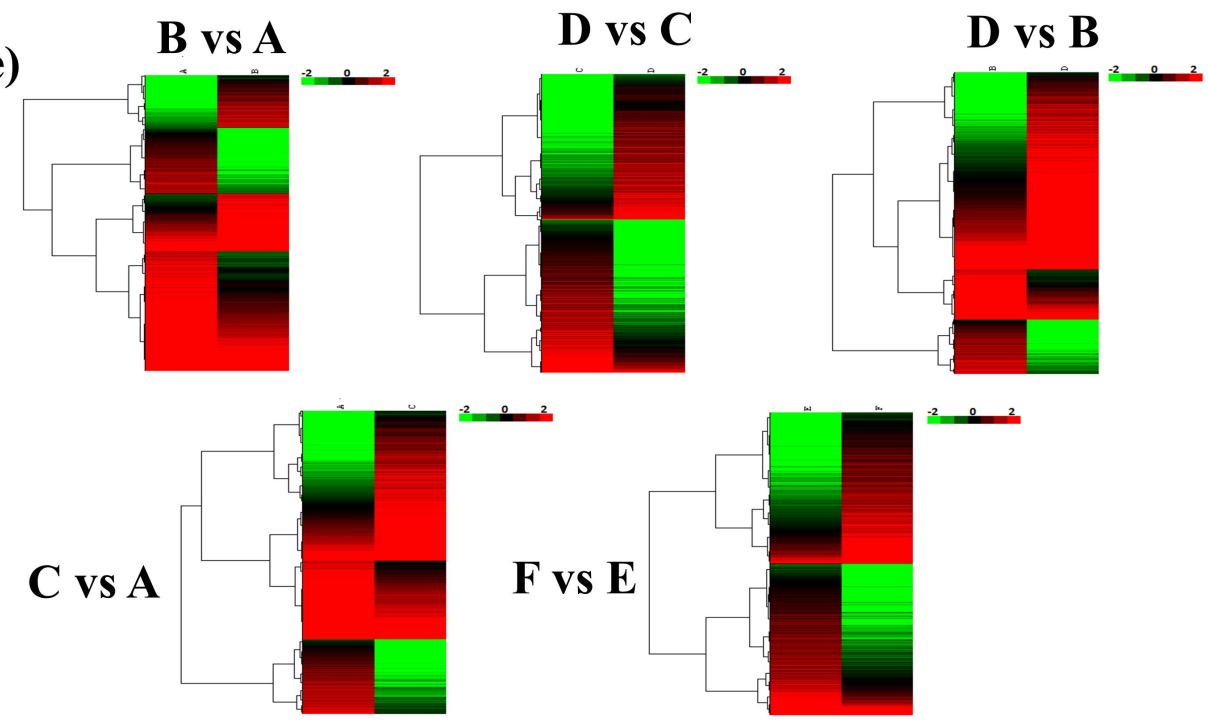

f)

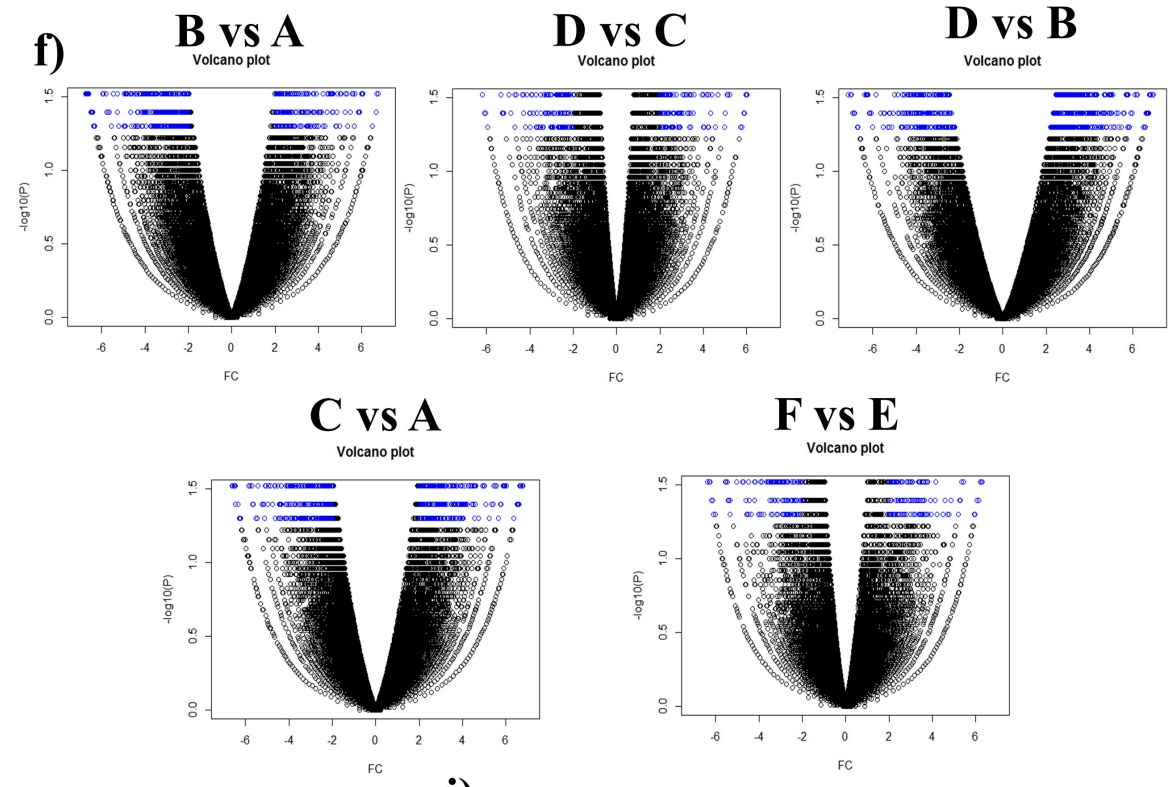

g)

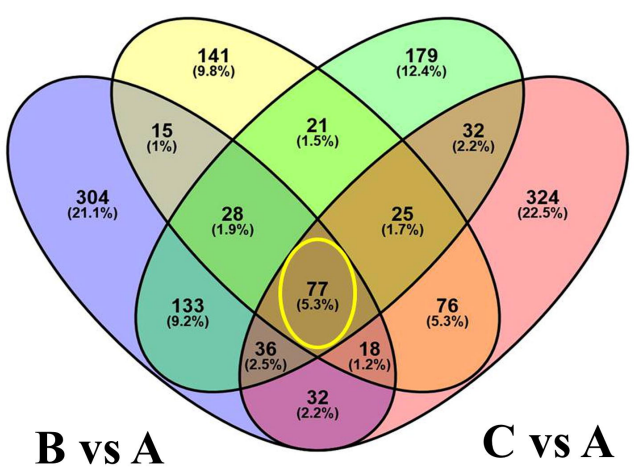

h)

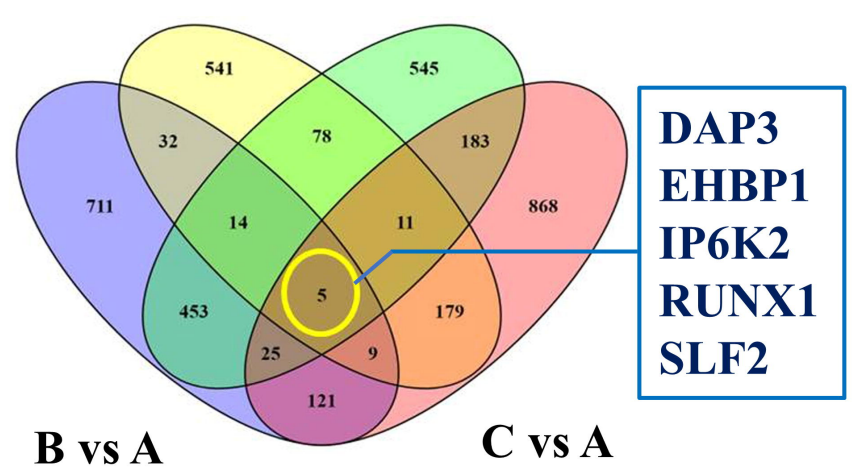

i)

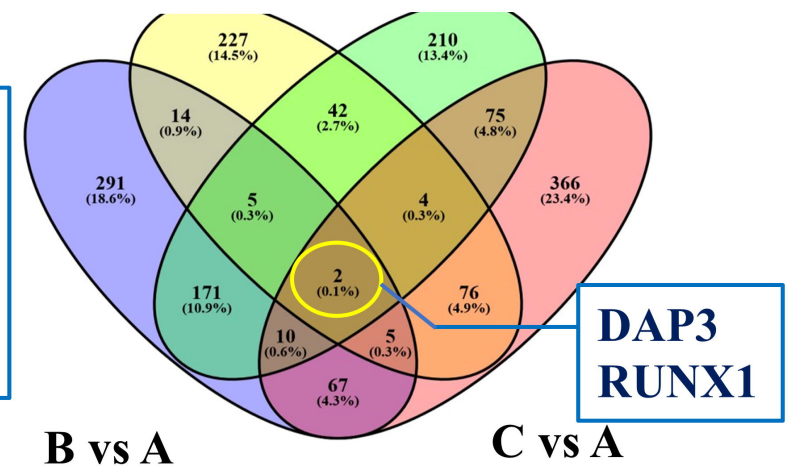

a)

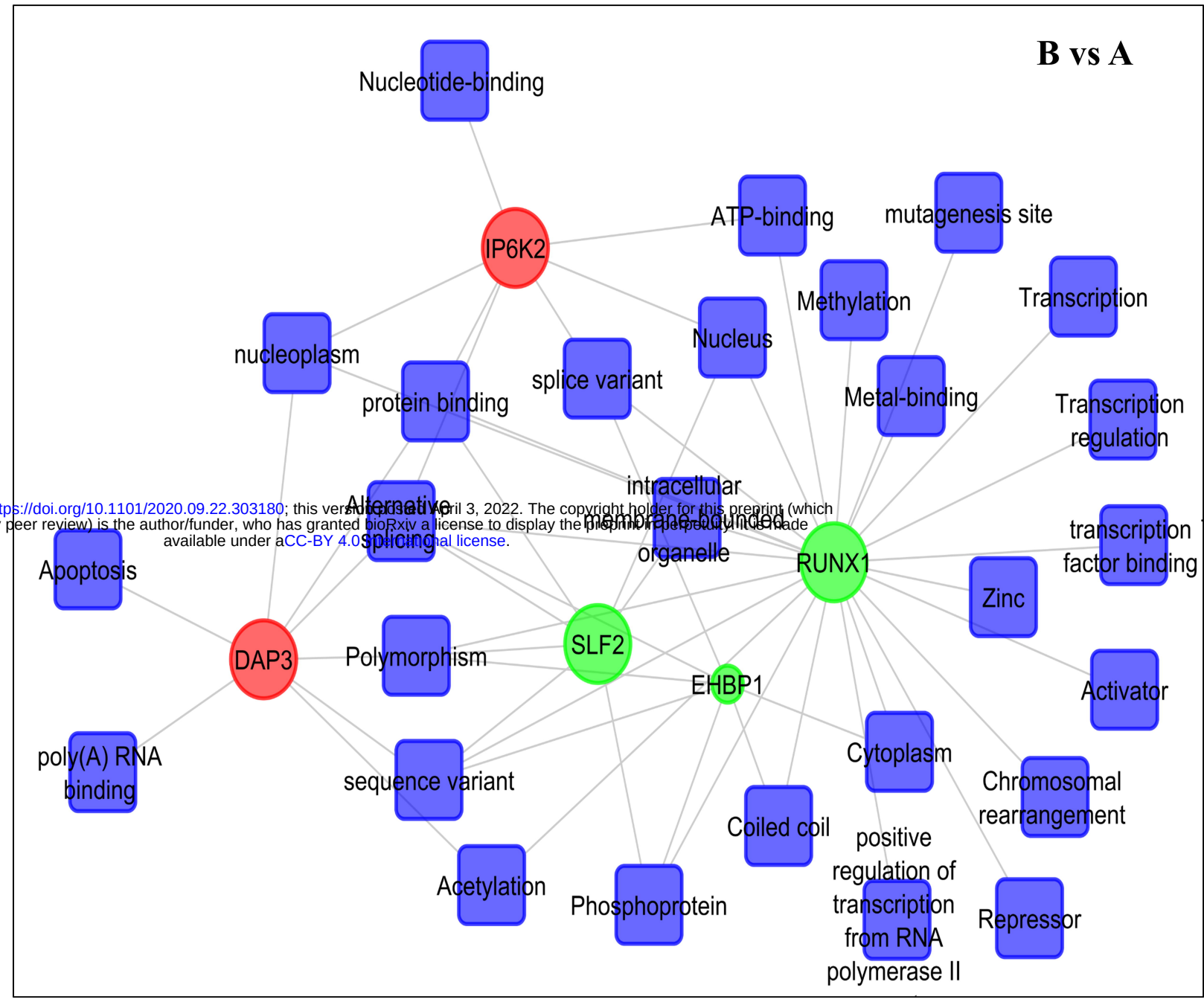

b)

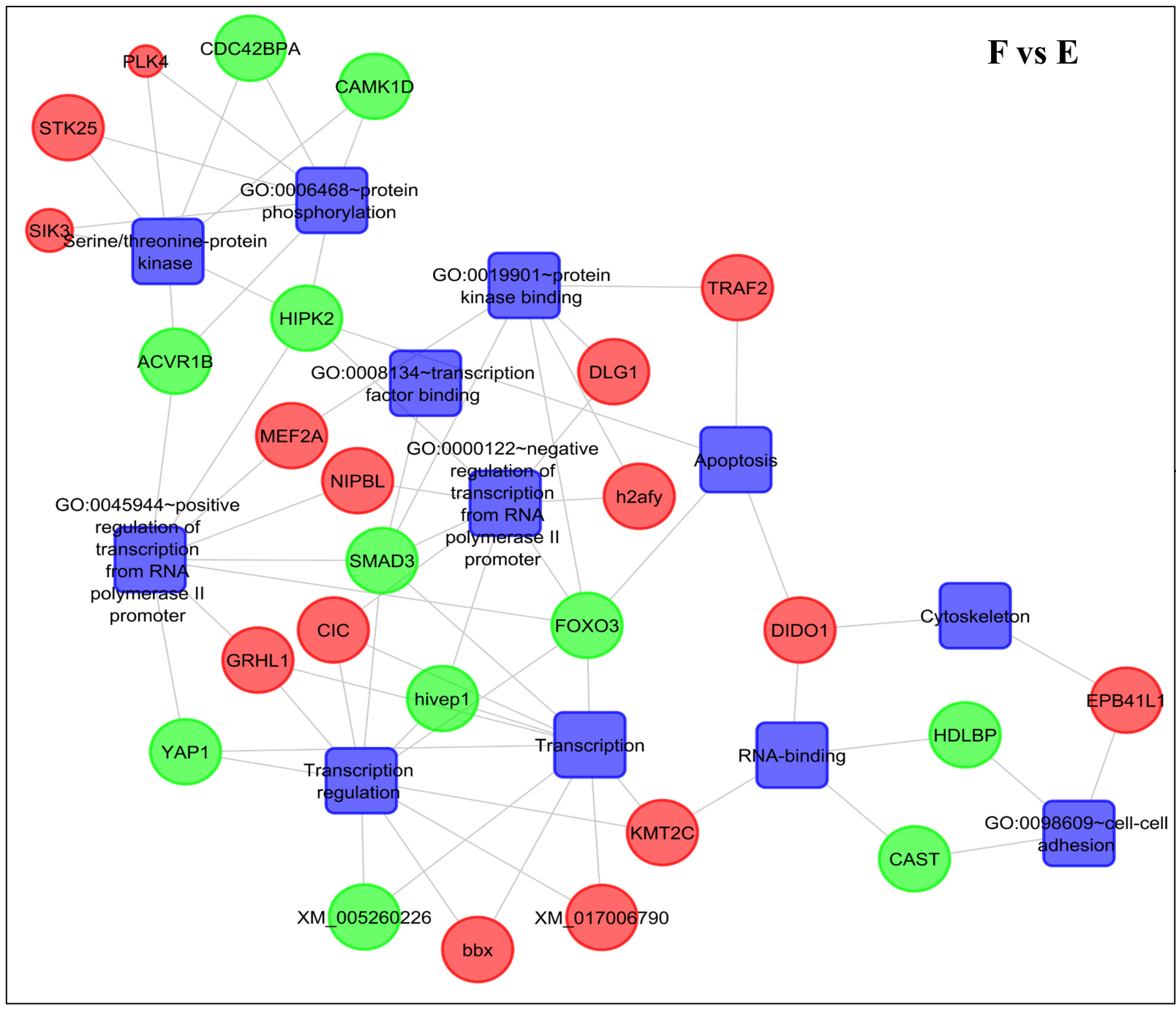

a)

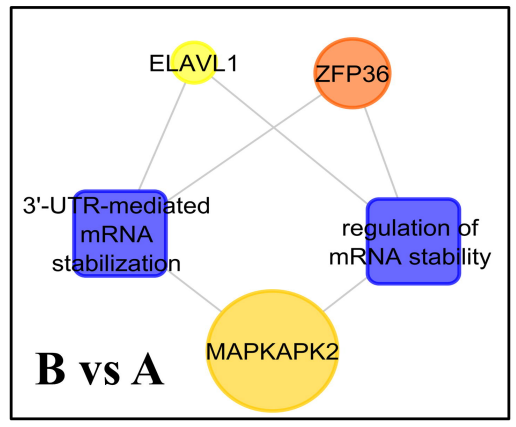

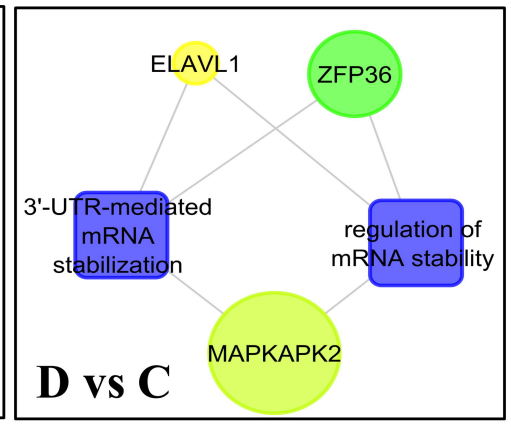

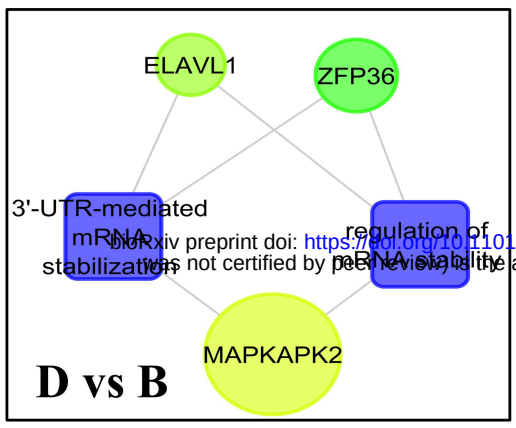

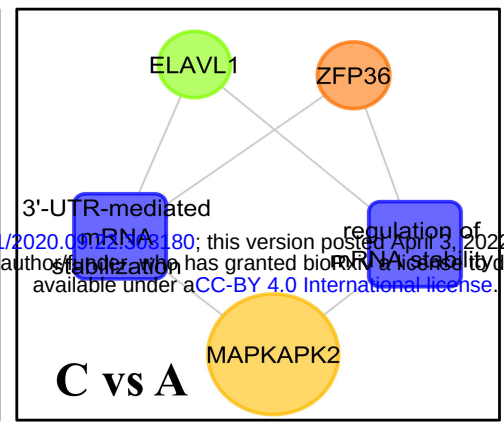

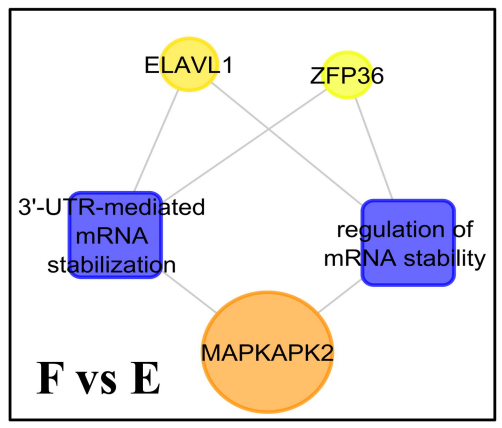

b)

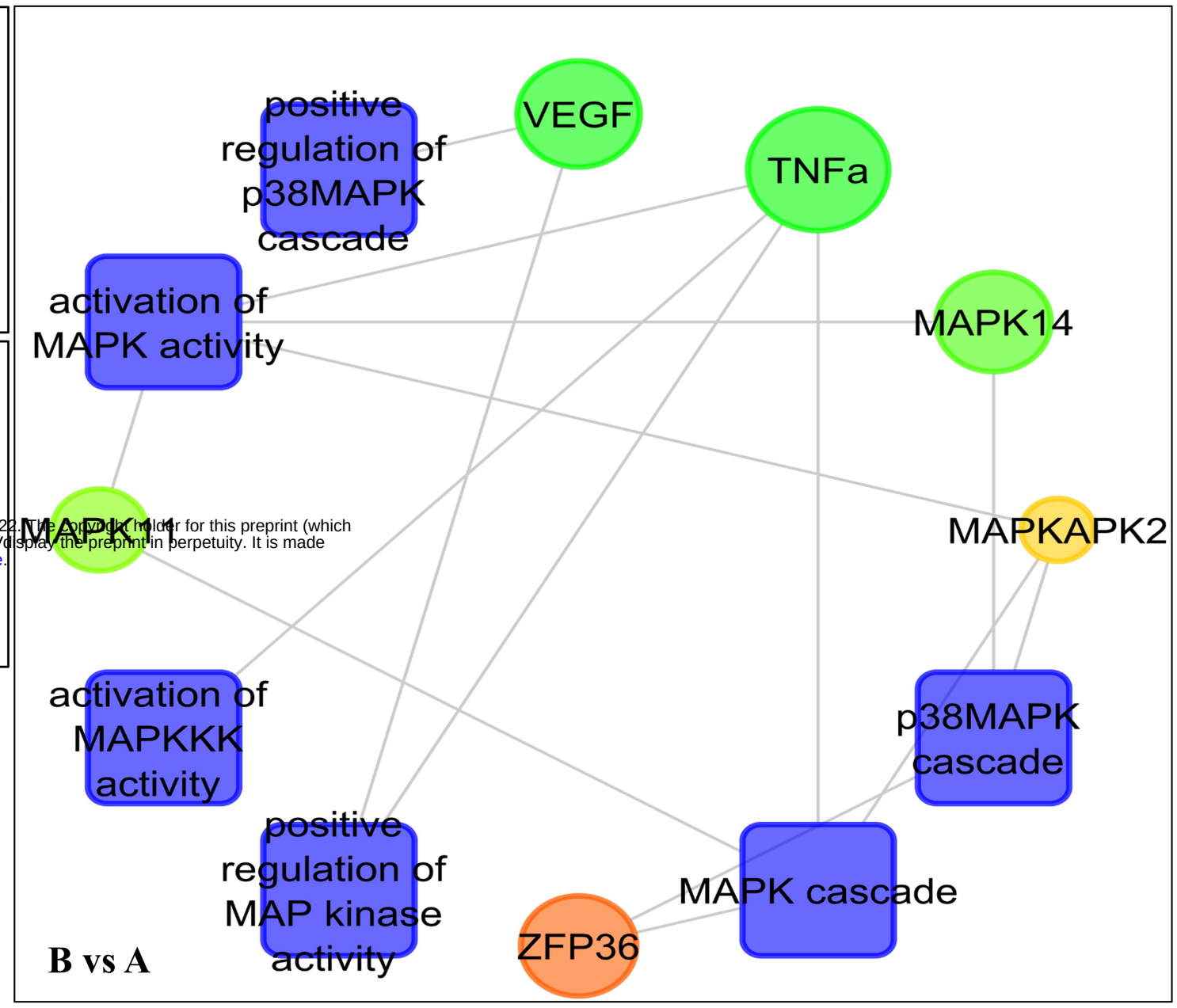

c)

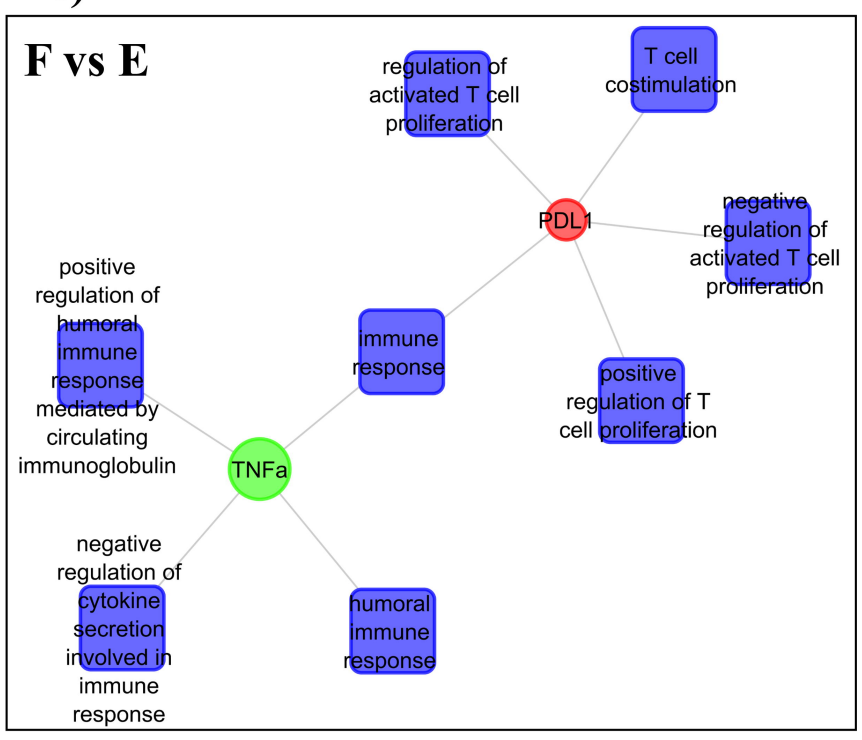

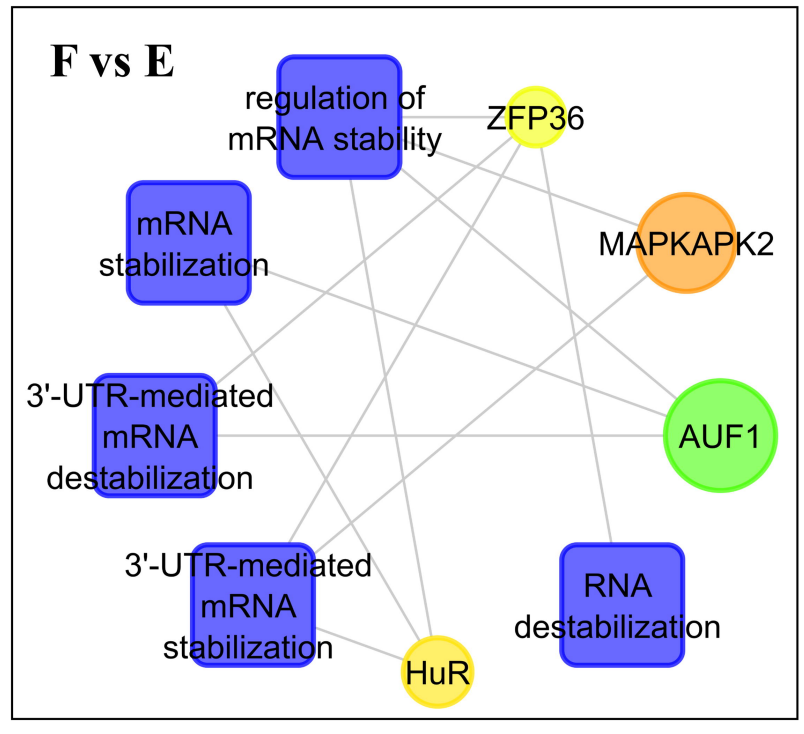

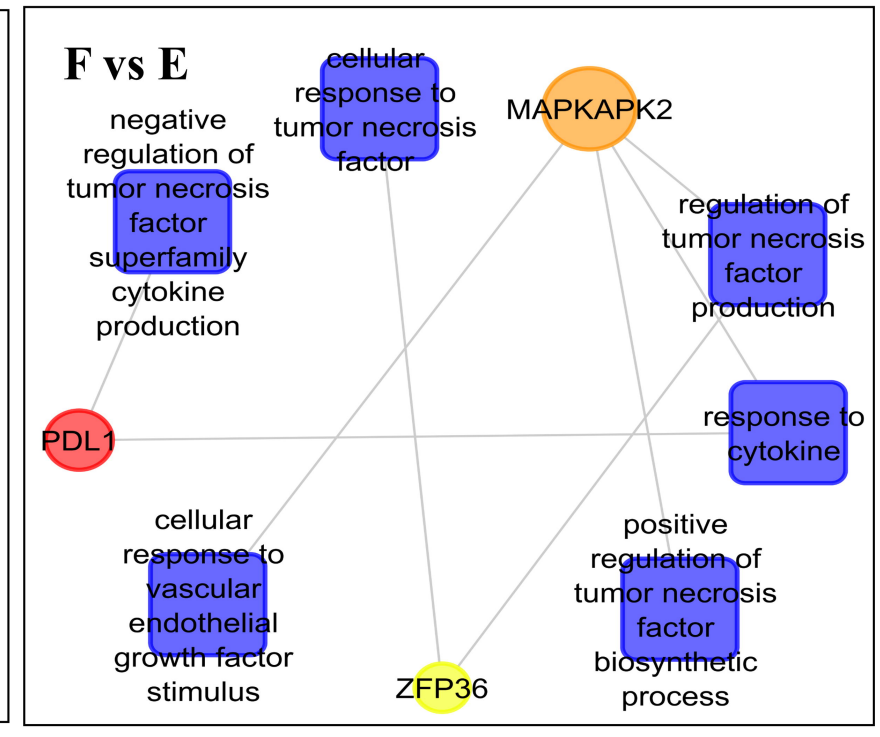

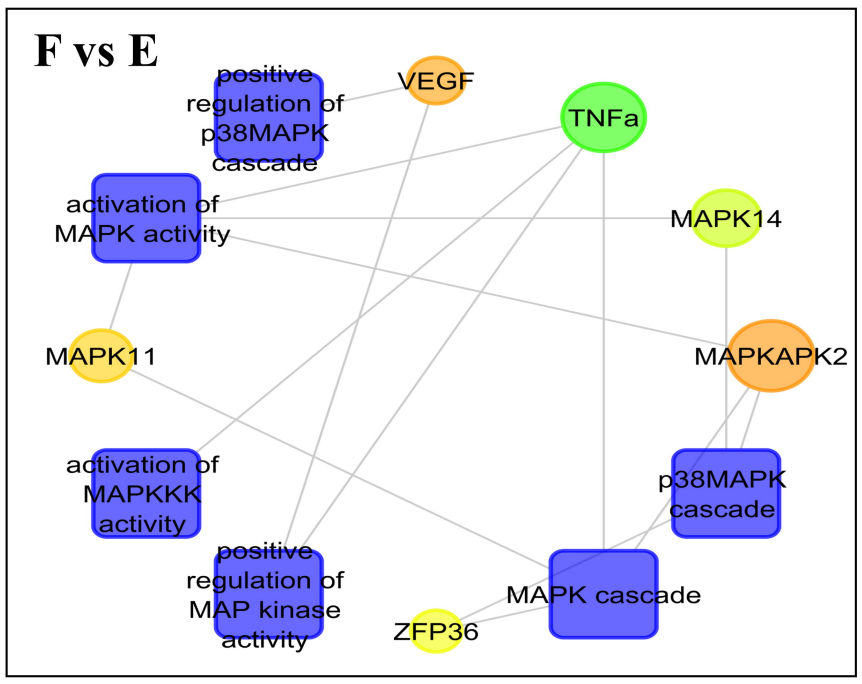

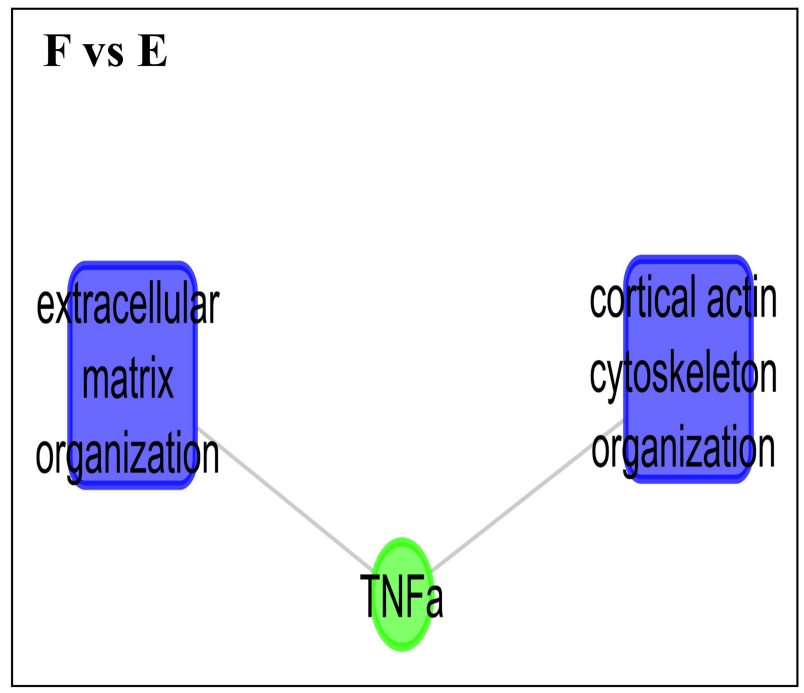

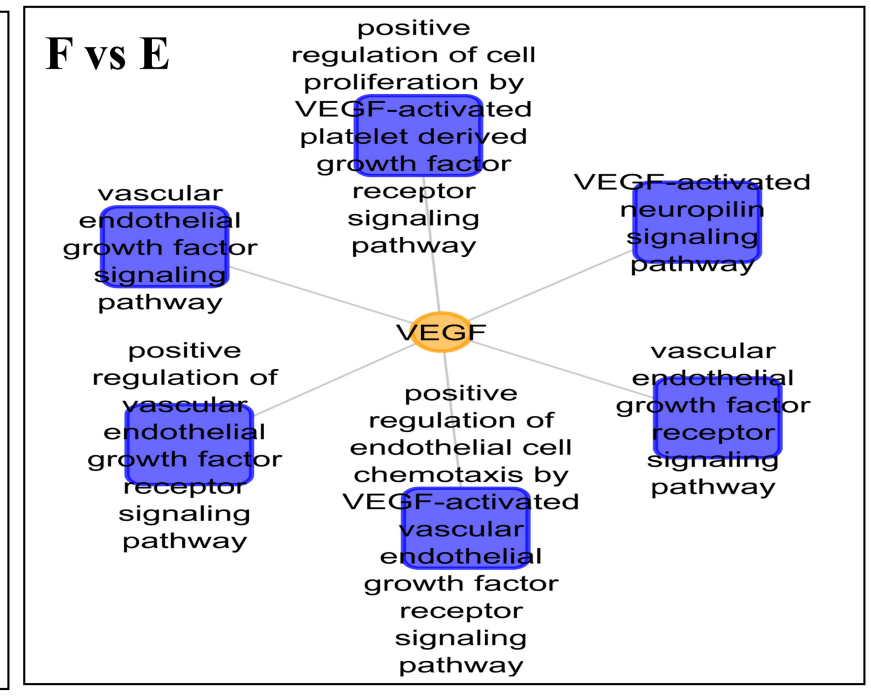

a)

Cell Line

16 Cancer specific biological processes

Xenograft

54 Cancer specific biological processes

- Found out the 3'-UTR regions of the transcripts.
- Found out the domain sequences of RBPs using **CISBP-RNA Database**
- Filtered out the transcripts that harbour RBP specific regions in their 3'-UTRs using **RBPmap**.

MK2-regulated transcripts that harbor RBP specific regions in their 3'-UTRs

b)

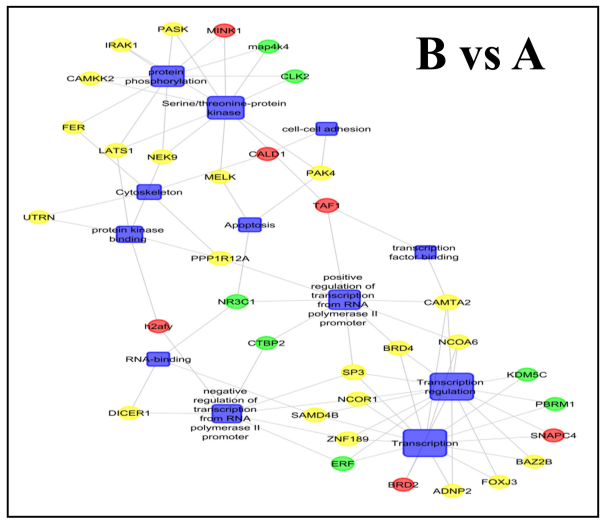

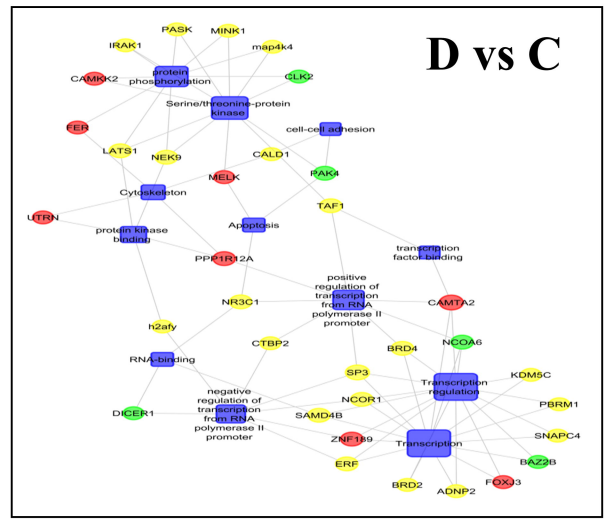

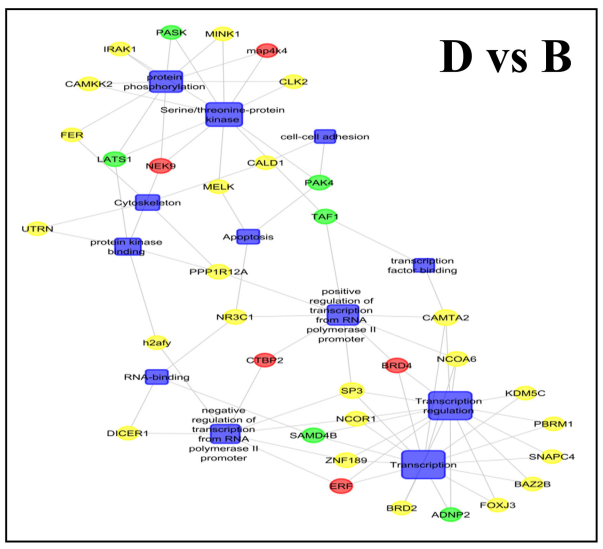

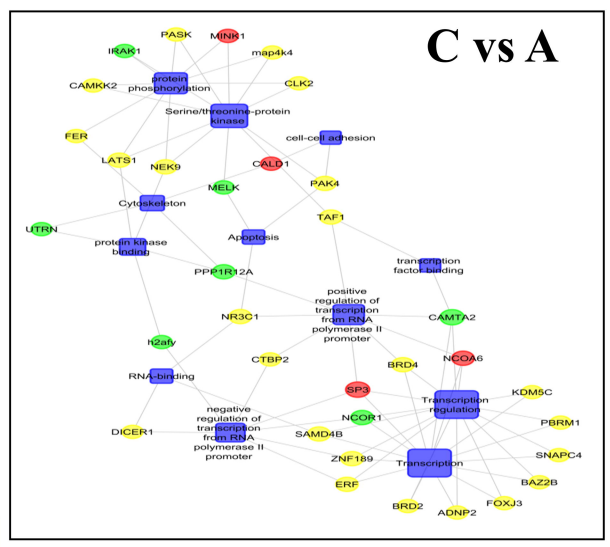

c)

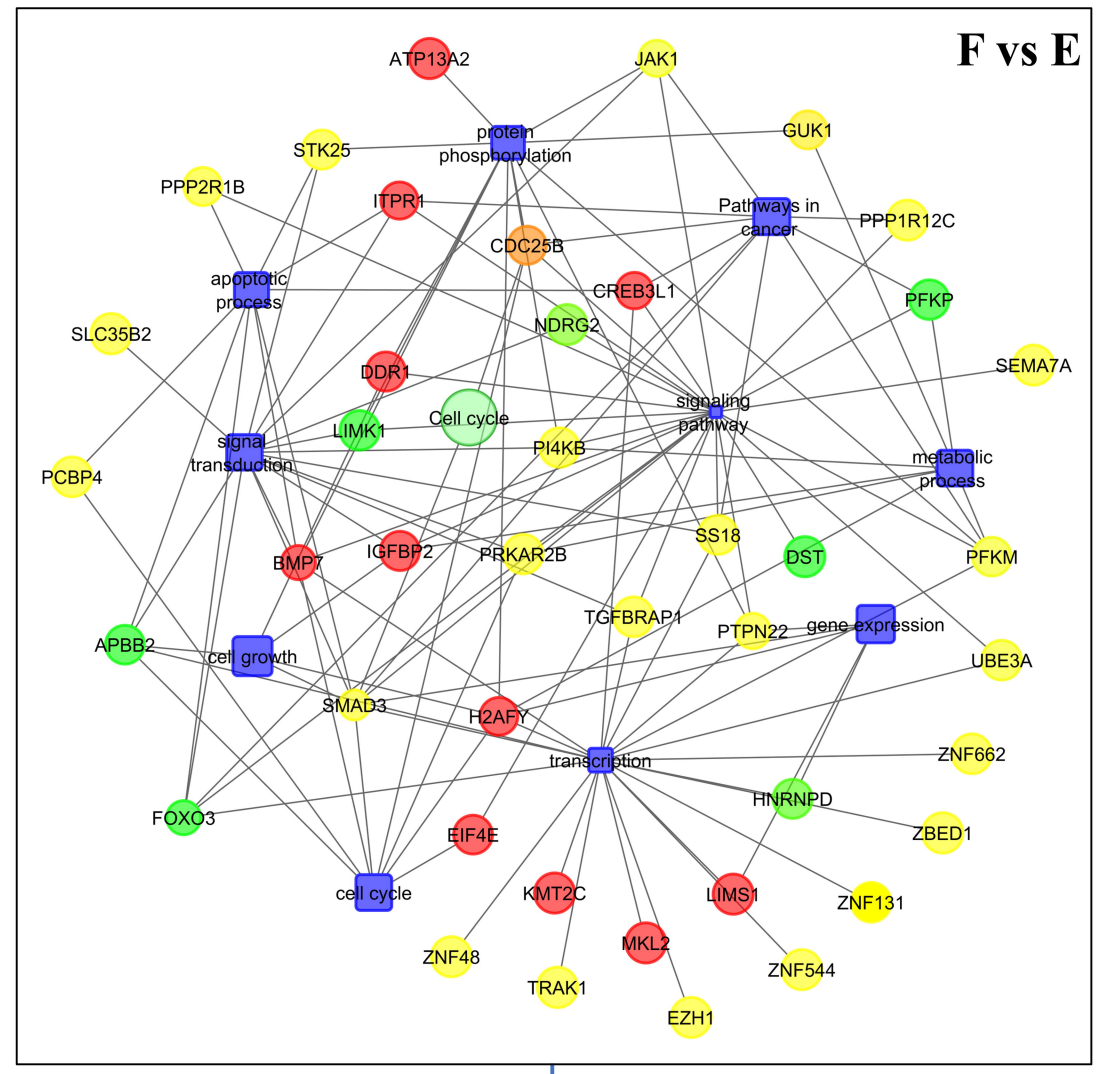

Cell Lines (A-D comparison)

34 MK2-regulated genes harboring RBP specific regions in their 3'-UTRs (Listed in Table 2)

Xenograft tumor (F vs E comparison)

48 MK2-regulated genes harboring RBP specific regions in their 3'-UTRs (Listed in Table 3)

a)

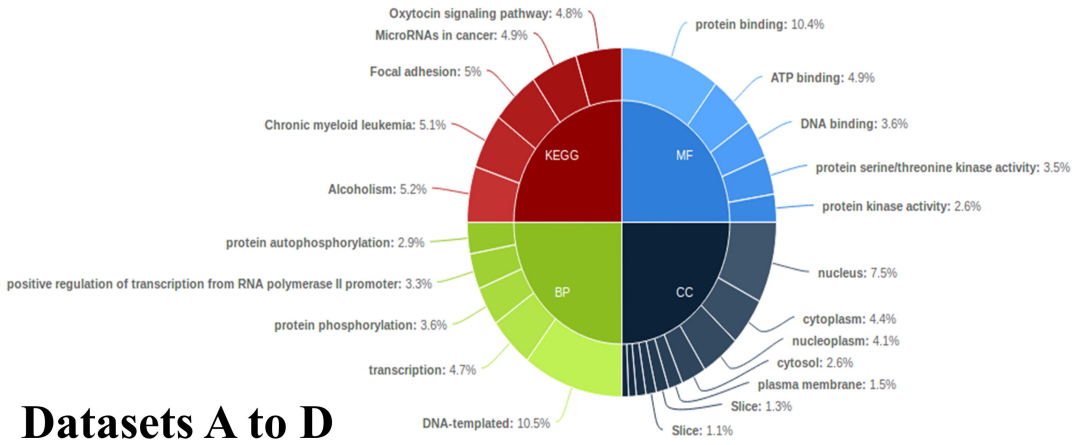

Datasets A to D

b)

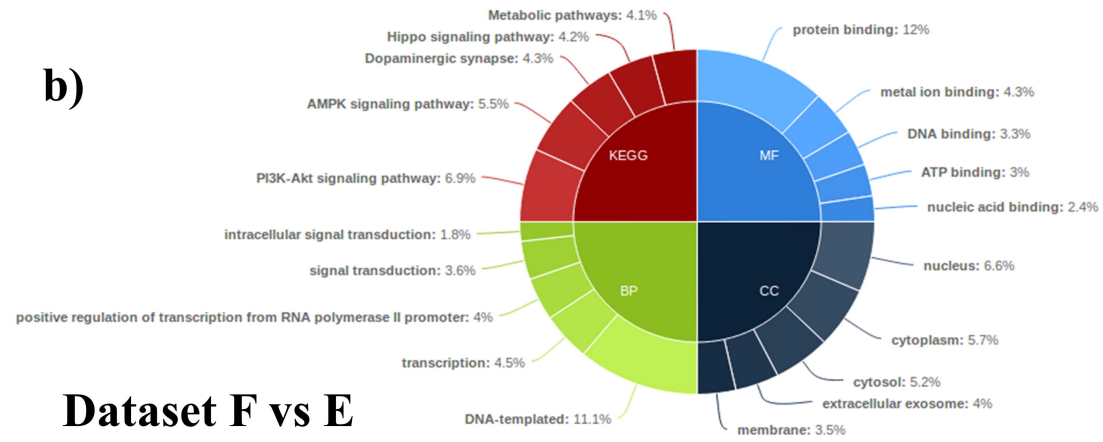

Dataset F vs E

c)

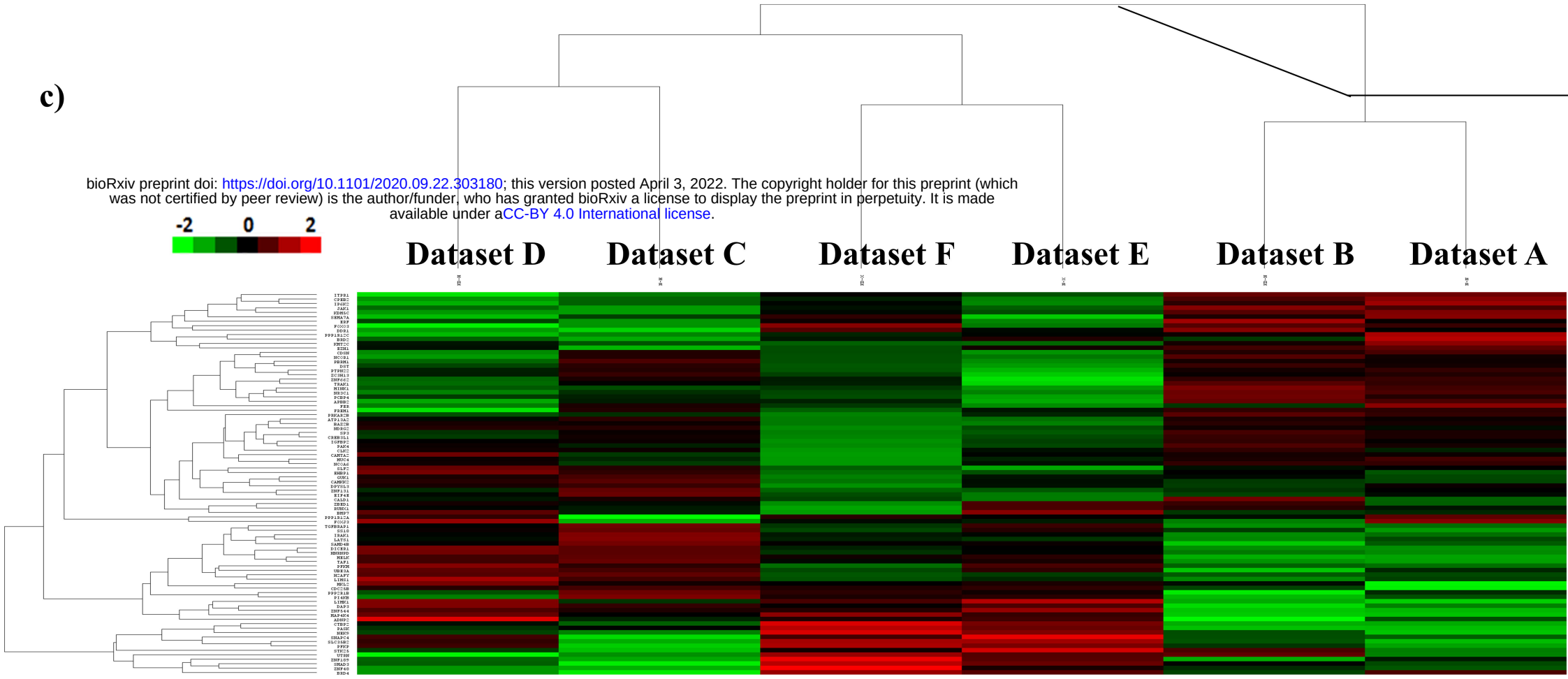

IGFBP2
PRKAR2B
MUC4
MELK
ZNF662
BMP7
CREB3L1

d)

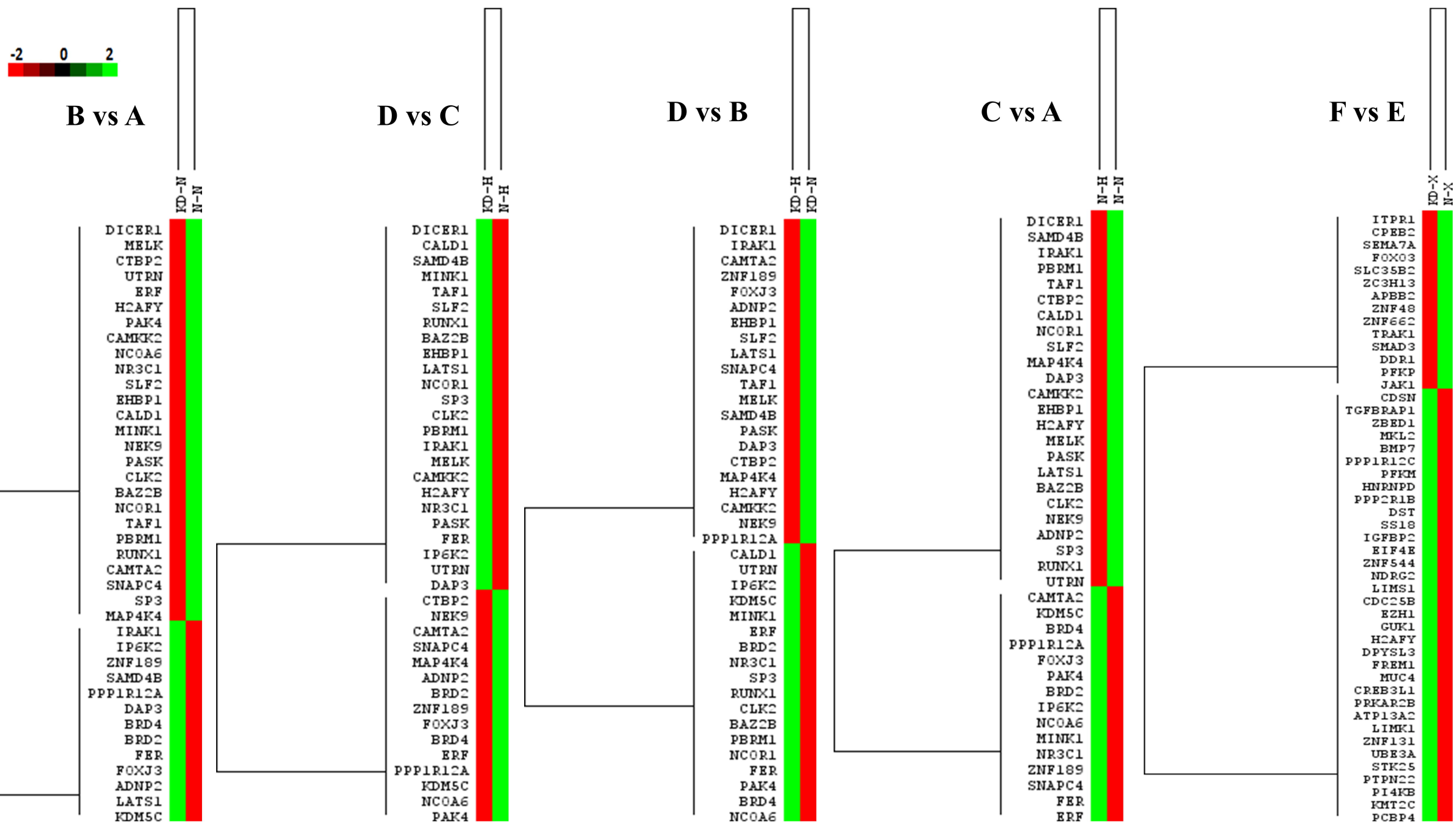

a)

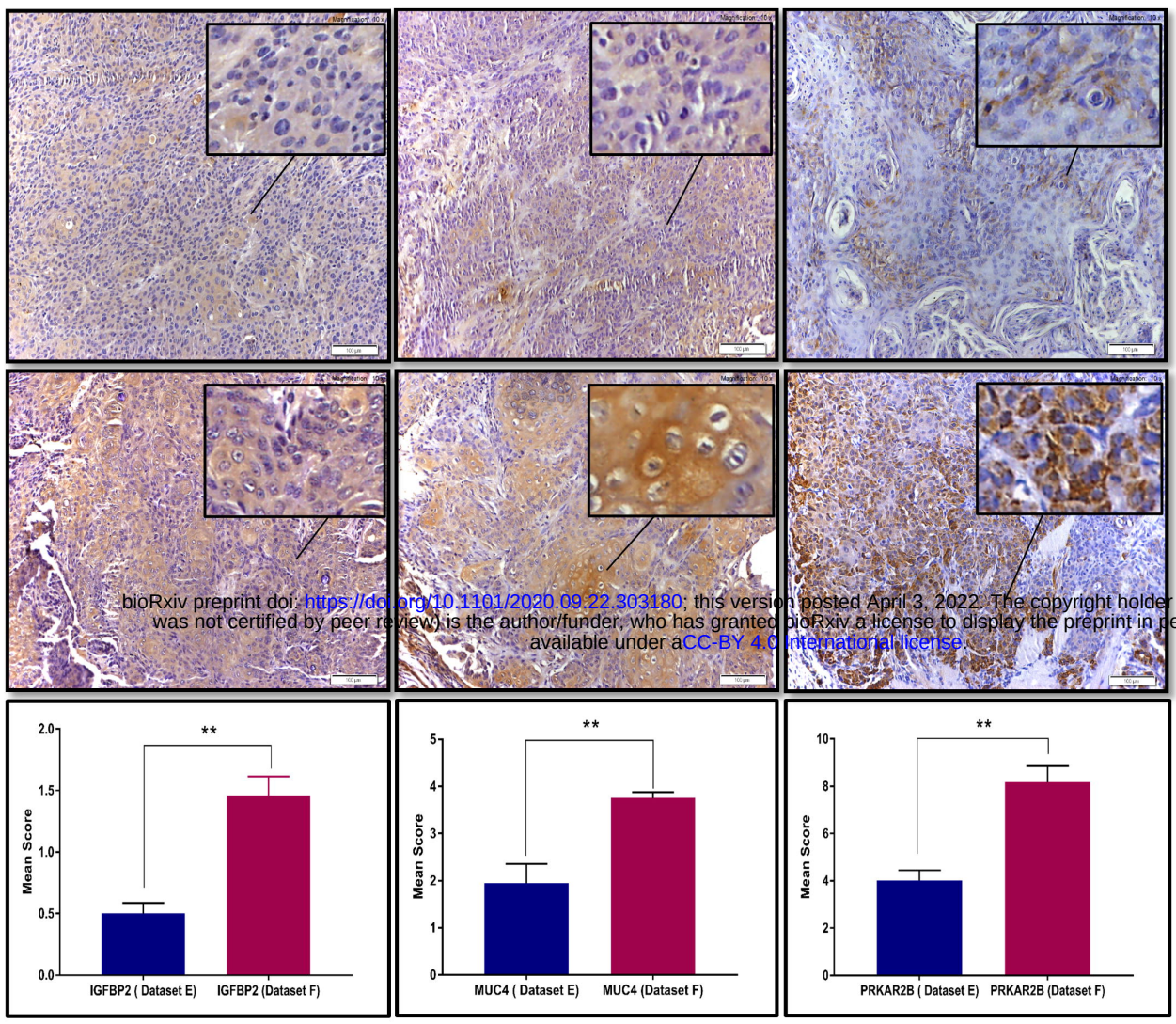

b)

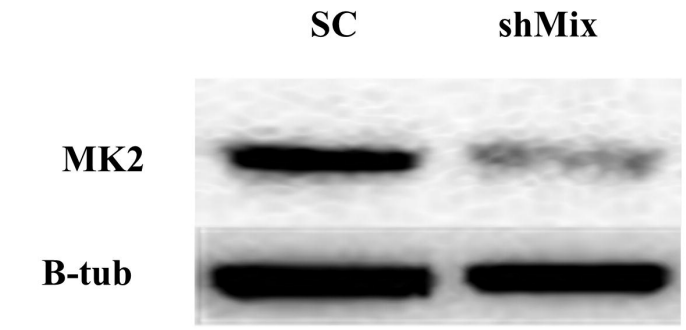

c)

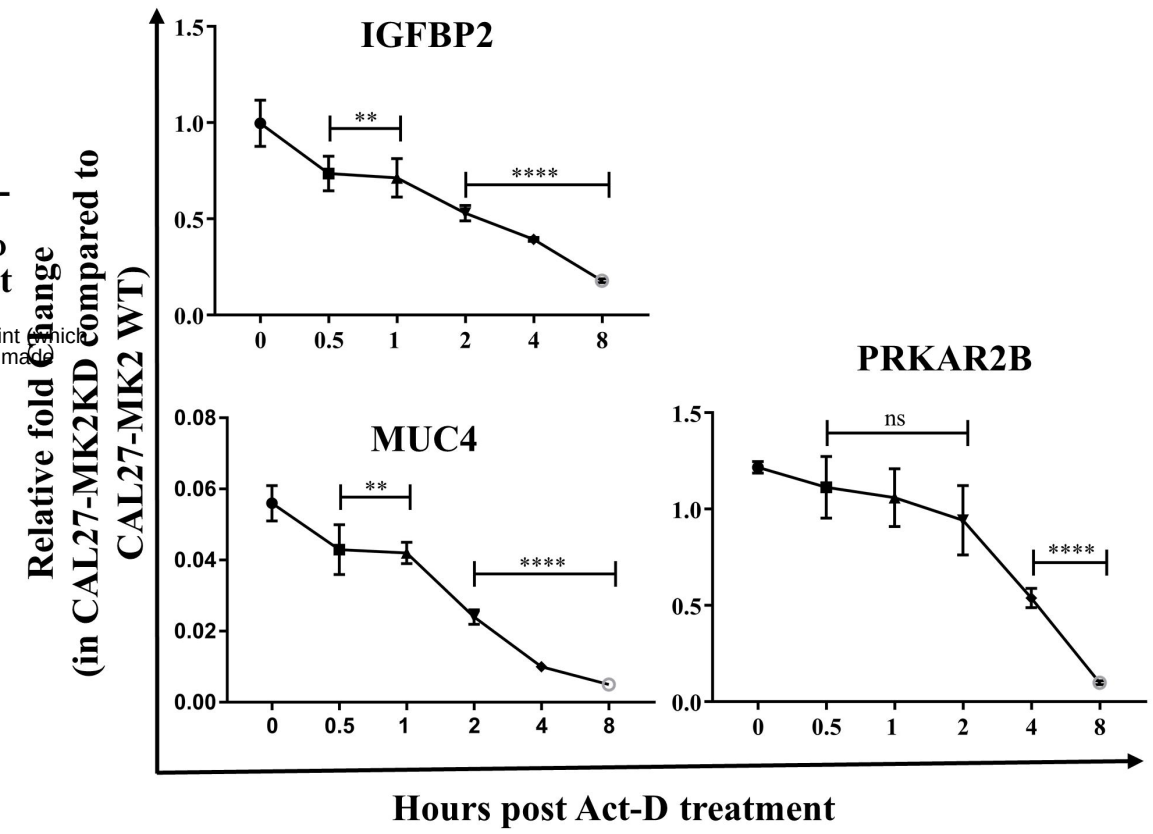

d)

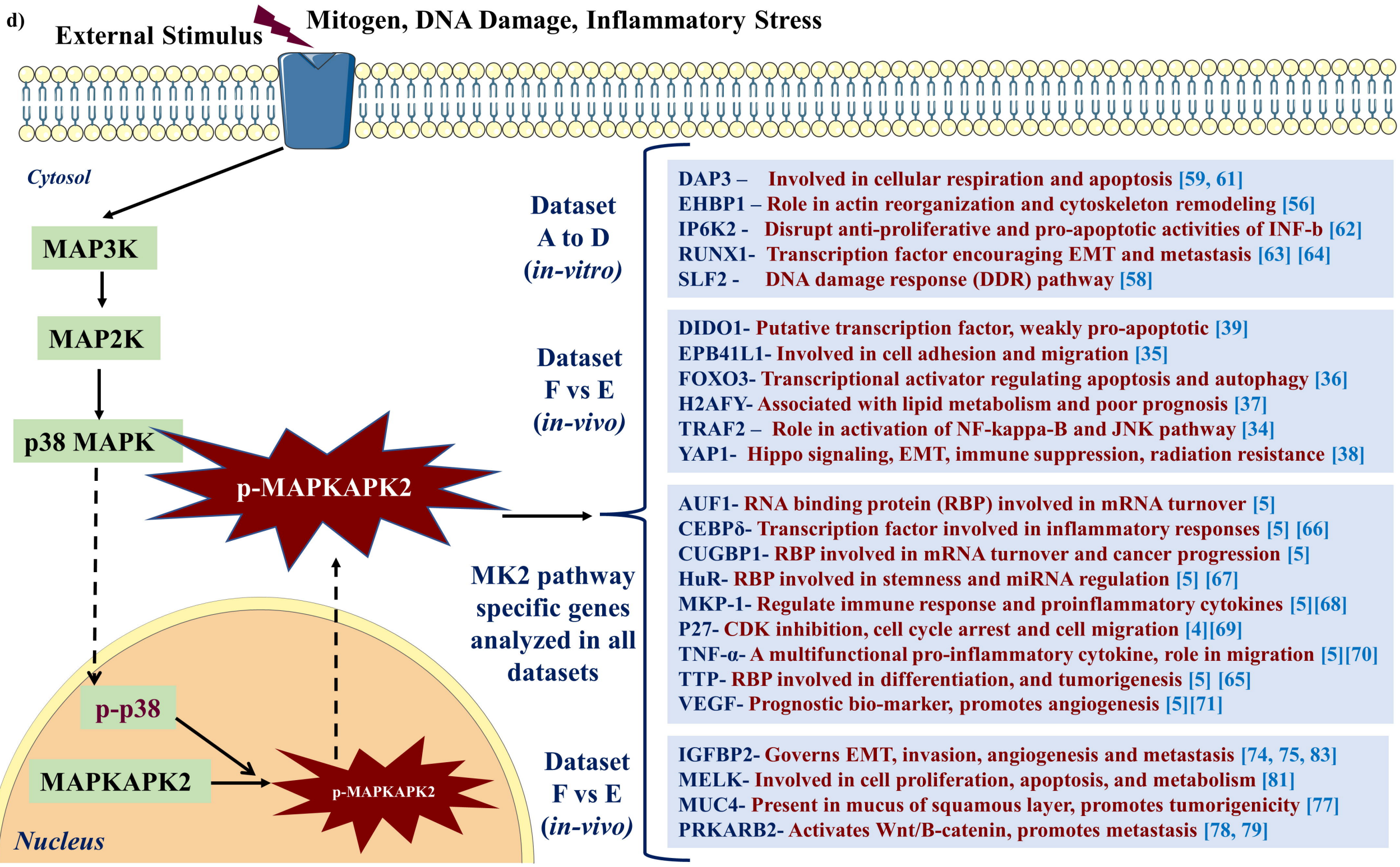

DAP3 – Involved in cellular respiration and apoptosis [59, 61]
EHBP1 – Role in actin reorganization and cytoskeleton remodeling [56]
IP6K2 - Disrupt anti-proliferative and pro-apoptotic activities of INF-b [62]
RUNX1- Transcription factor encouraging EMT and metastasis [63] [64]
SLF2 - DNA damage response (DDR) pathway [58]

DIDO1- Putative transcription factor, weakly pro-apoptotic [39]
EPB41L1- Involved in cell adhesion and migration [35]
FOXO3- Transcriptional activator regulating apoptosis and autophagy [36]
H2AFY- Associated with lipid metabolism and poor prognosis [37]
TRAF2 – Role in activation of NF-kappa-B and JNK pathway [34]
YAP1- Hippo signaling, EMT, immune suppression, radiation resistance [38]

AUF1- RNA binding protein (RBP) involved in mRNA turnover [5]
CEBPδ- Transcription factor involved in inflammatory responses [5] [66]
CUGBP1- RBP involved in mRNA turnover and cancer progression [5]
HuR- RBP involved in stemness and miRNA regulation [5] [67]
MKP-1- Regulate immune response and proinflammatory cytokines [5][68]
P27- CDK inhibition, cell cycle arrest and cell migration [4][69]
TNF-α- A multifunctional pro-inflammatory cytokine, role in migration [5][70]
TTP- RBP involved in differentiation, and tumorigenesis [5] [65]
VEGF- Prognostic bio-marker, promotes angiogenesis [5][71]

IGFBP2- Governs EMT, invasion, angiogenesis and metastasis [74, 75, 83]
MELK- Involved in cell proliferation, apoptosis, and metabolism [81]
MUC4- Present in mucus of squamous layer, promotes tumorigenicity [77]
PRKARB2- Activates Wnt/B-catenin, promotes metastasis [78, 79]